frontiers | Frontiers in Earth Science

TYPE Original Research
PUBLISHED 03 August 2023
DOI 10.3389/feart.2023.1164733

OPEN ACCESS

EDITED BY
Liang Zhang,
China University of Geosciences, China

REVIEWED BY
Yunlei Feng,
Hebei GEO University, China
Chaopeng Li,
Chinese Academy of Sciences (CAS), China

*CORRESPONDENCE
Min Wang,
qvfuwangmin@163.com

RECEIVED 13 February 2023
ACCEPTED 21 June 2023
PUBLISHED 03 August 2023

CITATION
Liu F, Wang M, Liu H and Ni R (2023), The Cenozoic spatiotemporal exhumation of the SE Tibetan Plateau: insight from the data mining and modeling of low-temperature thermochronology.
Front. Earth Sci. 11:1164733.
doi: 10.3389/feart.2023.1164733

The Cenozoic spatiotemporal exhumation of the SE Tibetan Plateau: insight from the data mining and modeling of low-temperature thermochronology

Fangbin Liu[1,2], Min Wang[1]*, Honghua Liu[3,4] and Ran Ni[1]

[1]School of Geography and Tourism, Qilu Normal University, Ji'nan, China, [2]Key Laboratory of Western China's Environmental Systems, Ministry of Education, College of Earth and Environmental Sciences, Lanzhou University, Lanzhou, China, [3]Key Laboratory of Geological Safety of Coastal Urban Underground Space, Ministry of Natural Resources, Qingdao, China, [4]Qingdao Geo-Engineering Surveying Institute, Qingdao, China

Introduction: The SE Tibetan Plateau is distinct from other margins due to its high elevation, long wavelength, and low relief. A clear understanding of the Cenozoic exhumation history of this region is the key to understanding the special geomorphological process and the associated mechanisms. Previous thermochronological studies have either focused on vertical sections or horizontal variations in the local regions. However, the spatiotemporal exhumation pattern of the entire SE Tibetan Plateau is enigmatic.

Methods: In this article, we have compiled 1,202 thermochronological data using joint kernel density estimation (KDE) and linear inversion approaches to address the exhumation process.

Results: The results reveal that at least six episodes of rapid cooling have occurred since the Cenozoic, which include ~61–58 Ma, 38–35 Ma, 32–23 Ma, 18–13 Ma, 11–6 Ma, and 4–3 Ma. Furthermore, the entire SE Tibetan Plateau underwent spatially inhomogeneous exhumation throughout the main episodes.

Discussion: We infer that all cooling episodes may be attributed to the lateral extrusion and continuous convergence between the Indian and Eurasian continents. Meanwhile, climate changes (e.g., intensified Asian summer monsoon and glacial processes) have also played a non-negligible role in shaping the landscape since the Miocene. Our results will provide new insights into geodynamic mechanisms of the exhumation processes throughout the whole SE Tibetan Plateau since the Cenozoic.

KEYWORDS

exhumation history, forcing mechanism, kernel density estimation, linear inversion, low-temperature thermochronology, SE Tibetan Plateau

1 Introduction

The collision between the Indian and Eurasian continental plates not only resulted in the creation of the Himalayan orogenic belt but also in the formation of the Tibetan Plateau, the roof of the world, with an average elevation of ~5,000 m above sea level (Fielding et al., 1994; Figure 1A). Cenozoic uplift and deformation of the Tibetan Plateau have a profound impact on the tectonic pattern of Eurasia (Molnar and Tapponnier, 1975; Tapponnier et al., 1981; Coleman and Hodges, 1995), as well as the global changing climate (Prell and Kutzbach, 1992; An et al., 2001). Understanding the Cenozoic evolution of the Tibetan Plateau is essential for exploring the geodynamic mechanisms and the interactions between tectonic deformation, climate change, and geomorphological evolution (Molnar et al., 1993; An et al., 2001; Molnar, 2005). However, details regarding when and how the uplift occurred and the uplift mechanisms of the Tibetan Plateau still remain controversial. The evidence of paleoaltimetry indicates that the elevation of the plateau is close to the present at the Late Eocene (Rowley and Currie, 2006; Polissar et al., 2009; Hoke et al., 2014). However, the rapid cooling and exhumation episode from thermochronology suggests that the onset of surface uplift spanned a relatively broad range from Late Paleocene to Early Eocene to Late Miocene (Turner et al., 1993; Coleman and Hodges, 1995; Clark et al., 2005; Ouimet et al., 2010; Wang E. et al., 2012; Dai et al., 2013; He et al., 2017; Nie et al., 2018). Furthermore, the models simulating the uplift mechanisms are disparate (Powell, 1986; Zhao and Morgan, 1987; Dewey, 1988; Houseman and England, 1993; Royden et al., 1997; Shen et al., 2001; Tapponnier et al., 2001); among these models, two end-member models have been often popularly proposed to explain the plateau growth, namely, the lateral extrusion model and lower crustal flow model. The lateral extrusion model suggests that the SE Tibetan Plateau was extruded along large strike-slip faults that are active during the early-to-mid-Cenozoic and attained its present height well before the Middle Miocene (Tapponnier et al., 2001). On the contrary, the lower crustal flow model infers that the topographic loading in the interior plateau underwent eastward expansion and resulted in the crustal thickening of the plateau margins since the Late Miocene (Royden et al., 1997; Clark and Royden, 2000).

As the frontier area of the plateau, the SE Tibetan Plateau is the key to understanding the aforementioned hot topics in geosciences. First, three of the largest Asian rivers, the Nu (Salween), Lancang (Mekong), and Jinsha (Yangtze), originate from this part of the plateau (Yang et al., 2016; Liu-Zeng et al., 2018a) (Figure 1). Therefore, its tectonic evolution is essential for understanding the formation of the Asian rivers. Second, the evolution of the East Asian monsoon is sensitive to the outward growth of the Tibetan Plateau (An et al., 2001). Therefore, when this part of the plateau reached its current elevation, it is critical to understand the driving mechanisms of the East Asian monsoon. Third, this part of the plateau is characterized by a gentle relief, in contrast to the steep change in elevation within a short distance from the northern, southern, and eastern margins (Hoke et al., 2014). Therefore, a clear Cenozoic uplift history of this part of the plateau is the key to testing the previous hypotheses regarding the deformation mechanisms. Particularly, this part of the plateau is considered an archetypal example of the lower crust

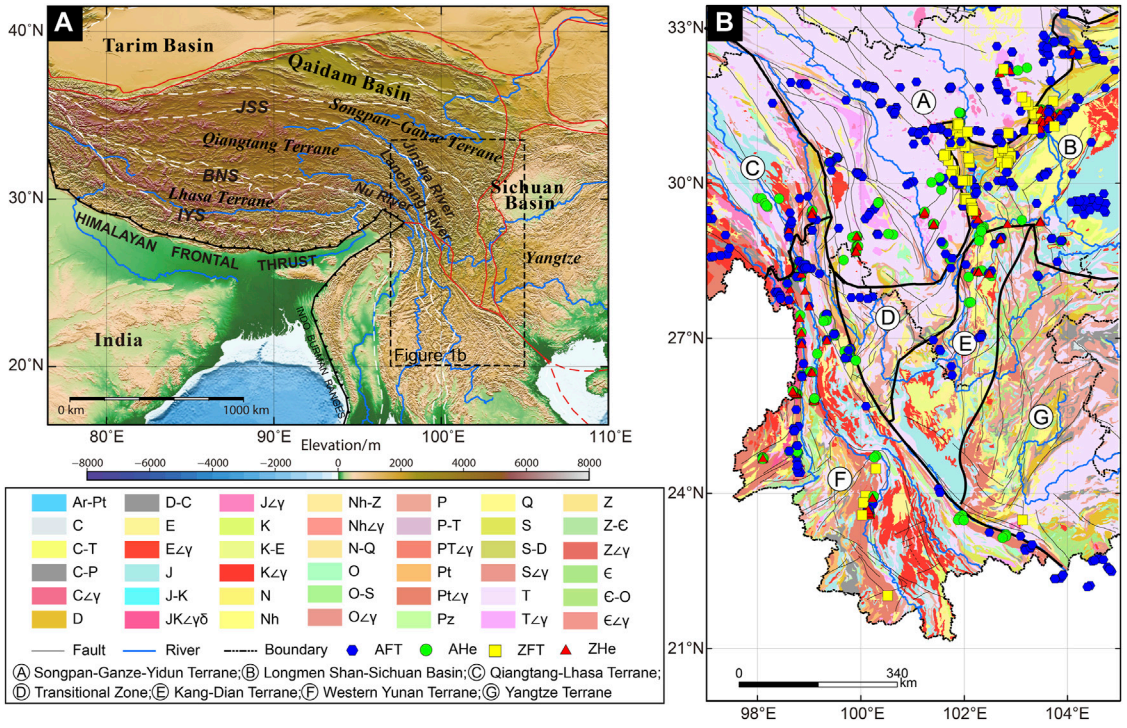

FIGURE 1
(A) Topographic and tectonic map in the Tibetan Plateau (data derived from https://github.com/gmt-china/china-geospatial-data/releases). The red lines represent the block boundaries. The white dotted lines are the suture zones. IYS, Indus-Yarlung suture; BNS, Bangong-Nujiang suture; JSS, Jinsha suture; **(B)** division of tectonic units in the SE Tibetan Plateau (after Burchfiel and Chen, 2012). Stratigraphic code [Q, Quaternary; N, Neogene; E, Paleogene; K, Cretaceous; J, Jurassic; T, Triassic; P, Permian; C, Carboniferous; D, Devonian; S, Silurian; O, Ordovician; ϵ, Cambrian; Pz, Paleozoic; Z, Sinian; Nh, Nanhuan; Pt, Proterozoic; Ar, Archeozoic; ∠γ, granite; ∠γδ, granodiorite].

flow hypothesis (Kirby et al., 2002; Clark et al., 2005), but this viewpoint contradicts the recent paleoaltimetry evidence (Hoke et al., 2014; Li S. et al., 2015; Wu et al., 2018).

Reconstruction of paleoaltimetry is the most straightforward way of restoring the elevation history of the Tibetan Plateau (Hoke et al., 2014; Li S. et al., 2015; Wu et al., 2018). However, to the best of our knowledge, data pertaining to the SE Tibetan Plateau are sparse. Recently, low-temperature thermochronology data are frequently used to infer the timing and magnitude of topographic relief change (Reiners, 2007; Cao et al., 2022); if interpreted correctly, these data directly measure rock exhumation instead of elevation. Therefore, these thermochronological data are not only complementary to paleoaltimetry data but also allow quantification of the exhumation histories of the plateau to a large extent (Reiners, 2007).

In the past decades, many studies have used low-temperature thermochronometry to investigate the rapid Cenozoic cooling and exhumation of the SE Tibetan Plateau. Most of these studies have either focused on orogen-perpendicular sections (Shen et al., 2016; Nie et al., 2018; Liu et al., 2021; Cao et al., 2022) or on lateral variations in the local regions (Deng et al., 2014; Tan et al., 2014). However, the spatiotemporal exhumation pattern of the entire SE Tibetan Plateau is enigmatic.

Hence, first, we investigated the role of tectonic and climatic processes since the Cenozoic exhumation of the SE Tibetan Plateau, based on the compiled 1,202 apatites (U-Th)/He (AHe), zircon (U-Th)/He (ZHe), apatite fission track (AFT), and zircon fission track (ZFT) ages together. Then, we established the timing episodes of exhumation for assessing the cooling age patterns by using kernel density estimation (KDE). Finally, a Gaussian linear inversion approach was used to constrain the spatiotemporal variation in the exhumation rates. Our findings provide new insight into the exhumation process in the entire SE Tibetan Plateau since the Cenozoic.

2 Geological setting

The SE Tibetan Plateau lies in Yunnan, western Sichuan, and Guizhou provinces of southwestern China (Figure 1). It consists of several lithospheric fragments, including Lhasa, Qiangtang, Songpan–Garze, South China, Baoshan, Lanping–Simao, and Indochina terranes from north to south (Burchfiel and Chen, 2012). This region experienced a complex and intense tectonic history, especially strike-slip faults linking to the intracontinental deformation, resulting from the India–Eurasia collision since the Cenozoic (Yin and Harrison, 2000). The strike-slip faults contain the Xianshui–Xiaojiang fault, Gaoligong Shan shear zone, Chongshan shear zone, Lancang fault, Ailao Shan–Red River shear zone, and Sagaing Fault. Among these, the right-lateral Gaoligong Shan and left-lateral Chongshan shear zones were active at 34–32 Ma (Wang et al., 2006; Akciz et al., 2008), while the activity of the Ailao Shan–Red River shear zone experienced a sinistral shear motion from 35 Ma to 17 Ma and right-lateral movement since ~5 Ma (Leloup et al., 1993; Gilley et al., 2003).

With respect to topographic features, the SE Tibetan Plateau is characterized by a high elevation, long wavelength, and low-relief landscape, which differs from the northern, southern, and eastern margins. Three of the largest Asian rivers, the Lancang River, Nu River, and Jinsha River, originate from this margin (Figure 1). These rivers flow more than thousands of kilometers and incise deep canyons up to 2–3 km (Clark et al., 2004), forming unique geomorphological units. In addition, it has been suggested that this low relief has been interpreted as a remnant of a continuous, low-altitude paleotopographic landscape prior to the uplift of the plateau (Clark et al., 2005). This remnant surface was preserved because the mainstem and the tributaries of the rivers had not yet penetrated the entire network. In contrast, Zhang et al. (2016) found that glacial erosion and ice edge weathering could have formed the aforementioned low-relief landform surface by studying glacial landforms in the study area, revealing the importance of glaciers in the formation of the surface of the plateau.

In recent decades, many scholars have carried out a large number of studies on its kinematics using different technologies, the most popular of which are paleomagnetism and GPS. For example, previous paleomagnetic studies have shown that the Sichuan–Yunnan Terrane has experienced clockwise rotational movements of ~10°–22° since the Paleocene, but counterclockwise movements of ~12°–15° occurred from the Miocene to Quaternary (Zhu et al., 2008; Lu et al., 2015). In the Baoshan Terrane, no significant tectonic rotational movements occurred until the Late Oligocene–Early Miocene, when it experienced ~80° clockwise rotations (Tong et al., 2016). Since the Pliocene, the Baoshan Terrane has undergone a counterclockwise rotational movement of ~15° (Pei et al., 2019). Similarly, the northern part of the Lamping–Simao Terrane has undergone ~80° clockwise rotational motion, accompanied by 638 ± 792 km of southward motion (Yang X. et al., 2020). However, others suggested that the Indochina Terrane has undergone a 20°–35° clockwise rotation since the Late Oligocene, and the Simao Terrane has undergone an overall clockwise rotation of ~35°, with 400–800 km of southward extrusion (Yang et al., 1995; Tong et al., 2013; Gao et al., 2015; Tsuchiyama et al., 2016).

Although paleomagnetism is an important tool for analyzing paleotectonic deformation, GPS observations are mainly used to reveal the distribution of present-day tectonic deformation and its underlying mechanisms. Previous studies show that the direction of present-day crustal motion along the SE Tibetan Plateau generally undergoes a clockwise rotation along the Eastern Himalayan syntaxis (Wang and Shen, 2020).

To summarize, considering long-time scales, the SE Tibetan Plateau has experienced southward extrusion over hundreds of kilometers since the Cenozoic, accompanied by large-angle clockwise rotational motion, as revealed by GPS measurements.

3 Materials and methods

3.1 Compiled data

To reconstruct the complete exhumation history of the SE Tibetan Plateau, we compiled 1,202 low-temperature thermochronological data from previous studies throughout the study area, including AHe (n = 260), ZHe (n = 182), AFT (n = 633), and ZFT (n = 127) (Figures 1B, 2). All of these ages are considerably younger than the corresponding stratigraphic or crystallization ages, which is a reflection of the post-depositional or monotonous cooling histories of the basement rocks. It should be noted that we only consider the Cenozoic cooling and exhumation

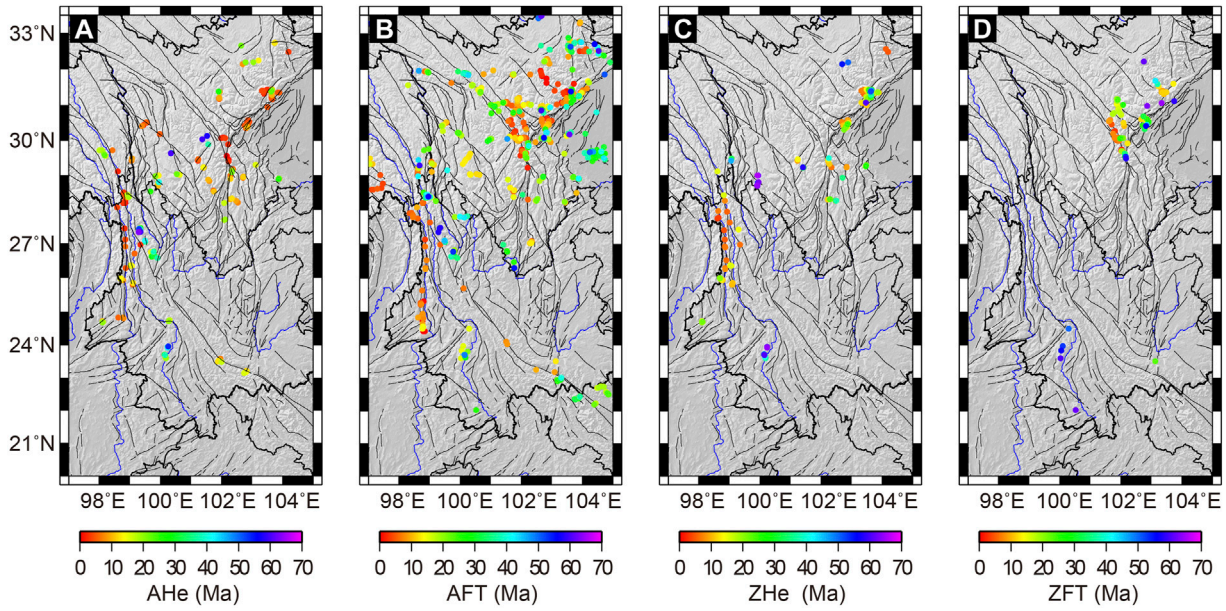

FIGURE 2
Compilation of low-temperature thermochronometric ages from the SE Tibetan Plateau. **(A)** AHe data; **(B)** AFT data; **(C)** ZHe data; **(D)** ZFT data.

of the SE Tibetan Plateau. Ages older than 64 Ma are not employed for the qualitative investigation of cooling age patterns and inverse modeling as they provide little information (e.g., Herman et al., 2013; Fox et al., 2016; Jiao et al., 2017; Willett et al., 2020). Furthermore, we split the area into seven major terranes/units based on geological formations (Figure 1A; Burchfiel and Chen, 2012) and sample distribution, which include Songpan–Ganze–Yidun, Longmen Shan–Sichuan Basin, Qiangtang–Lhasa, transitional zone, Kang-Dian, Western Yunnan, and Yangtze (Figure 1B). Of these, we have not collected low-temperature thermochronological data for the Yangtze, so we focus our analysis on the other six tectonic units.

3.2 Kernel density estimation

KDE is a non-parametric method for calculating the probability density function of random variables. KDE is a continuous and smooth substitute for the standard histogram. KDE is a function that uses intrinsic adaptive bandwidth to account for analytical uncertainty and overlays a Gaussian "bell curve" on top of each measurement. These adaptive functions eliminate the uncertainties generated by analytical errors and age abundance by adjusting the bandwidth dependent on the local density. Vermeesch (2012) provided a detailed explanation about KDE. Therefore, it will not be repeated in this paper.

3.3 Set up of the inversion model and selection of parameters

For the quantitative assessment of the spatiotemporal exhumation pattern of the SE Tibetan Plateau, we employed a Gaussian linear inversion approach based on compiled AHe, ZHe, AFT, and ZFT ages. This inversion approach was established by Fox et al. (2014). We adopted the updated version described in Herman and Brandon (2015). This approach exploits the exhumation rates from age-elevation sections, as well as multiple thermochronological systems with different closure temperatures (Fox et al., 2014). According to this approach, depth (Z_c), from the closure isotherm/depth to the surface, is defined as the integral of exhumation rates ($\dot{e}$) over a finite number of time intervals, from the cooling age (τ) to the present day. The equation is represented as follows:

$$Z_c = \int_0^{\tau} \dot{e} dt. \tag{1}$$

For providing a numerical solution for Eq. 1, we need to discretize the time integral before parameterizing the exhumation rate as a piecewise constant function. The subsequent is as follows:

$$\sum_{i=1}^{N-1} \dot{e}_j \Delta t + \dot{e}_N R = Z_c, \tag{2}$$

where $\dot{e}_j$ represents the average exhumation rate within uniform time intervals (Δt). N is the number of intervals, R is the remainder of the division of τ by N-1, and R = τ-(N-1)Δt.

However, the model assumes that the rocks experience monotonic cooling histories and do not account for the reburial process (i.e., negative exhumation rates). Hence, Eq. 1 could be converted to a logarithmic space to prevent this situation:

$$\zeta = \ln\left(\int_0^{\tau} \exp(\varepsilon) dt\right), \tag{3}$$

where $\zeta = \ln(Z_c)$ and $\varepsilon = \ln(\dot{e})$.

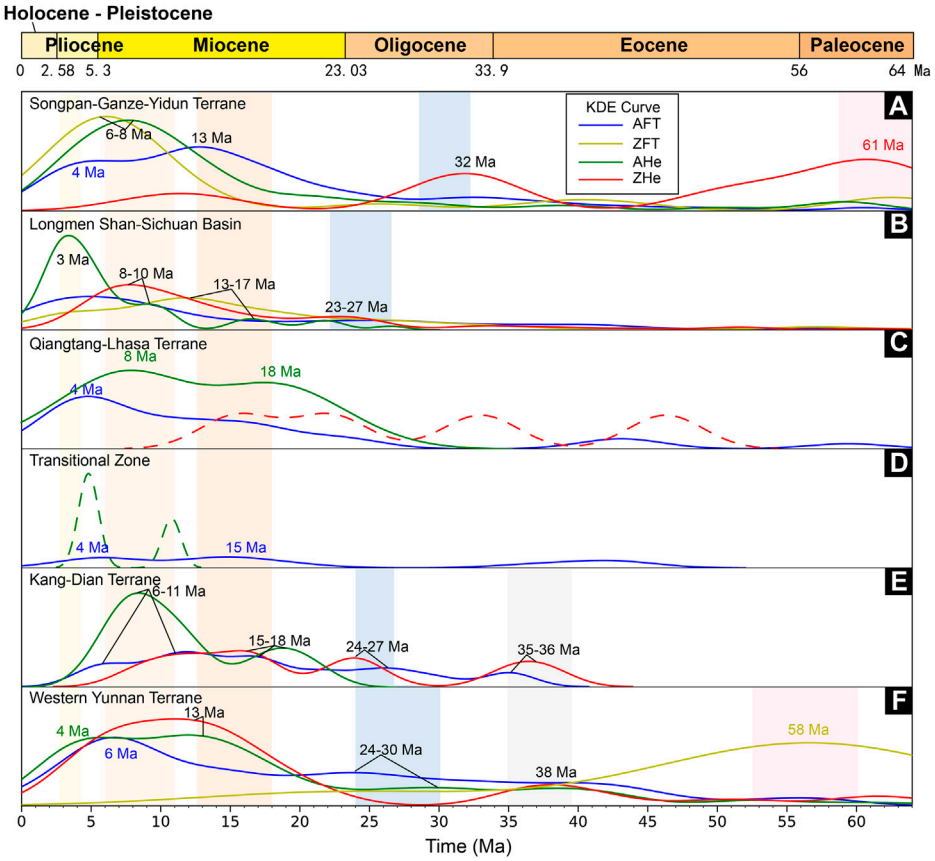

FIGURE 3
KDE results of different tectonic units in the SE Tibetan Plateau. **(A)** Songpan-Garze-Yidun Terrane; **(B)** Longmen Shan-Sichuan Basin; **(C)** Qiangtang-Lhasa Terrane; **(D)** Transitional Zone; **(E)** Kang-Dian Terrane; **(F)** Western Yunnan Terrane.

The parameter $\dot{e}$ or ε in the equations is an unknown quantity, and solving the linear inversion is required. Therefore, we provide *a priori* exhumation rate ($\dot{e}_{pri}$) and obtain an estimate of the variance about this mean (σ^2). Hence, the *a priori* model covariance matrix is built using this variance:

$$C_M(i,j) = \sigma^2 \exp\left(-\left(\frac{d}{L}\right)^2\right). \quad (4)$$

The matrix $C_M(i,j)$ is constructed for each time interval containing the horizontal distance (d) between the *i*th and *j*th samples, and L represents a specified correlation length.

Finally, a non-linear least square method is used to solve the exhumation rate by employing multiple iterations:

$$\varepsilon_{m+1} = \varepsilon_m - \mu\left(C_M G^t C_D^{-1}(\zeta_m - \zeta_{obs}) + (\varepsilon_m - \varepsilon_{pri})\right), \quad (5)$$

where m is the iteration number, ε_{pri} is the logarithm of the initial value as the *a priori* exhumation rate ($\dot{e}_{pri}$), G is the product of the exponential of ε and time interval divided by the closure depth (Herman and Brandon, 2015), C_D is the data covariance matrix, μ is an arbitrarily chosen parameter which controls how rapidly the model parameters change, and ζ_m and ζ_{obs} are the logarithms of the modeled and observed closure depths, respectively.

As the exhumation history obtained from the inversion may depend on the chosen priori exhumation rate, we used various values of the parameters, such as its variance, the initial geothermal gradient, the spatial correlation length, and the time intervals, to test the robustness of our results (Supplementary Table S1). A total of five inverse models are depicted in Supplementary Table S2, which is provided as a supplementary material. The M_1 model, which provides the optimal solution out of these models, is the one on the basis of which the results have been interpreted. The detailed interpretation is described in Section 5.1. In the M_1 model, we used a prior exhumation rate of 0.1 ± 0.1 km/Myr, a correlation length scale of 20 km (Yang et al., 2016), and a time interval length of 4 Myrs, from 64 Ma to the present. The tested prior exhumation rate is the end-member value for the regions that exhibit higher exhumation rates like the Jianchuan Basin (0.06 km/Myr before Early Cenozoic; Cao et al., 2020). Both a spatial correlation length and time interval act as trade-off parameters between solution resolution in space and the need to smooth the noise (Yang et al., 2016). A larger correlation length will always increase the numerical values of the resolution and decrease the variance, whereas the time interval number will always decrease the resolution (Willett et al., 2020). Therefore, it is necessary to choose the aforementioned suitable values for simulation. In addition, we also set a fixed model thickness of

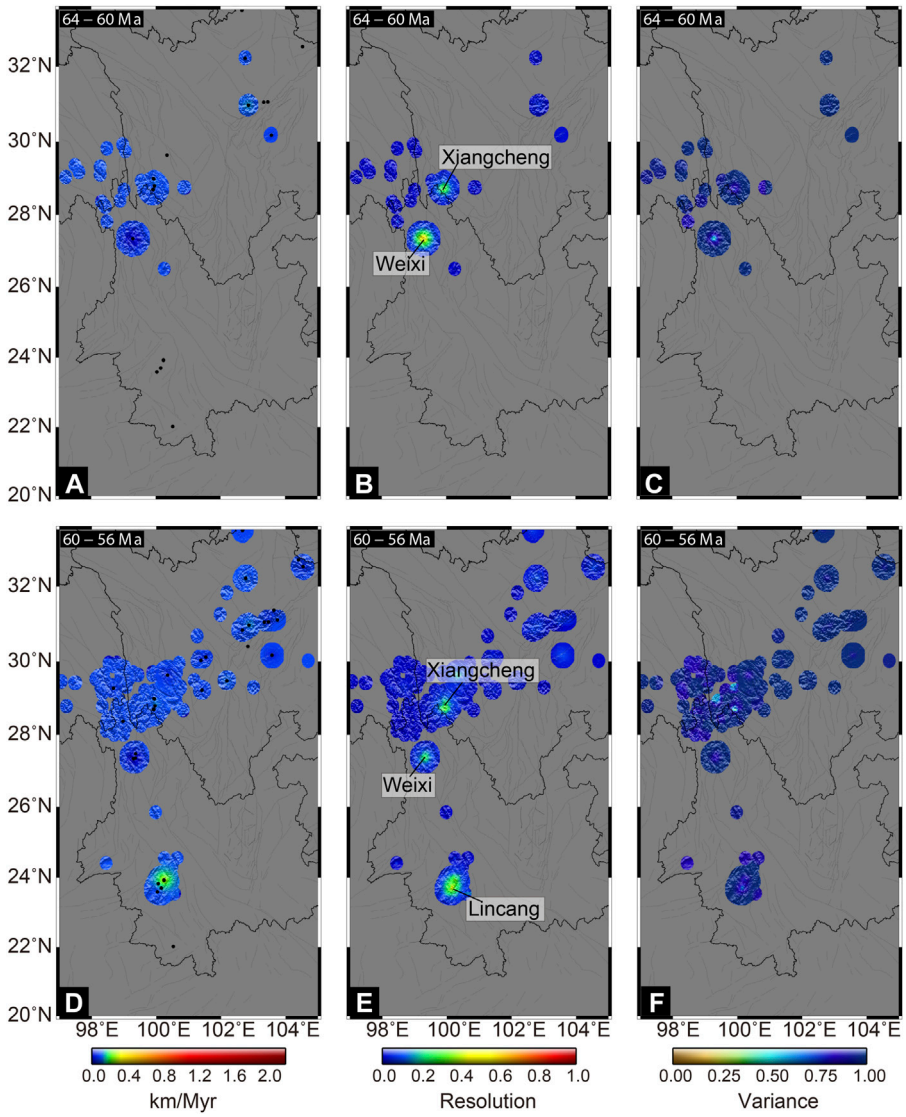

FIGURE 4
Results of the inversion during the Paleocene. **(A)** Exhumation rates, **(B)** Resolution, and **(C)** Variance of 64–60 Ma; **(D)** Exhumation rates, **(E)** Resolution, and **(F)** Variance of 60–56 Ma.

30 km with a temperature value of 10°C at the surface (Liu et al., 2021; Shen et al., 2021), which produces an initial geothermal gradient of 30°C/km (Yang et al., 2016). The thermal diffusivity is 25 km^2/Myr (Braun et al., 2012), and heat production is not considered; as reported by Batt and Braun (1997), the curvature of the geotherm caused by heat-producing elements can be neglected while interpreting low-temperature thermochronology.

4 Results

4.1 Time and episodes of rapid exhumation of the SE Tibetan Plateau during the Cenozoic

The 1,202 available low-temperature thermochronological data were statistically analyzed using KDE with various terranes/units in order to clarify the full exhumation signals of the SE Tibetan Plateau. This analysis ultimately produced a multi-peak distribution of age patterns (Figure 3). Of these, a total of 307 data pertained to the Songpan–Ganzi–Yidun Terrane, revealing five peaks (Figure 3A): 61 Ma (ZHe), 32 Ma (AFT/ZHe), 13 Ma (AFT/ZHe), 8–6 Ma (ZFT/AHe), and 4 Ma (AFT). Furthermore, 478 data pertained to the Longmen Shan–Sichuan Basin, with four population peaks since the Oligocene (Figure 3B), including 27–23 Ma (AHe/ZHe), 17–13 Ma (ZFT/AHe), 10–8 Ma (AHe/ZHe), and 3 Ma (AFT/AHe). With respect to the Qiangtang–Lhasa Terrane, AHe data revealed two Miocene age peaks at 18 Ma and 8 Ma, while the AFT ages revealed one population cluster at 4 Ma (Figure 3C). In contrast, the sample size of the transitional zone is even smaller, with only 13 data (AFT = 10 and AHe = 3); thus, only the AFT data were statistically analyzed, and based on previous studies, it was concluded that two peaks existed in this area, at ~15 Ma and ~4 Ma (Clark et al., 2005; Lai et al., 2007; Zou et al., 2014; Figure 3D). Furthermore, 46 data pertaining to the Kang-Dian Terrane

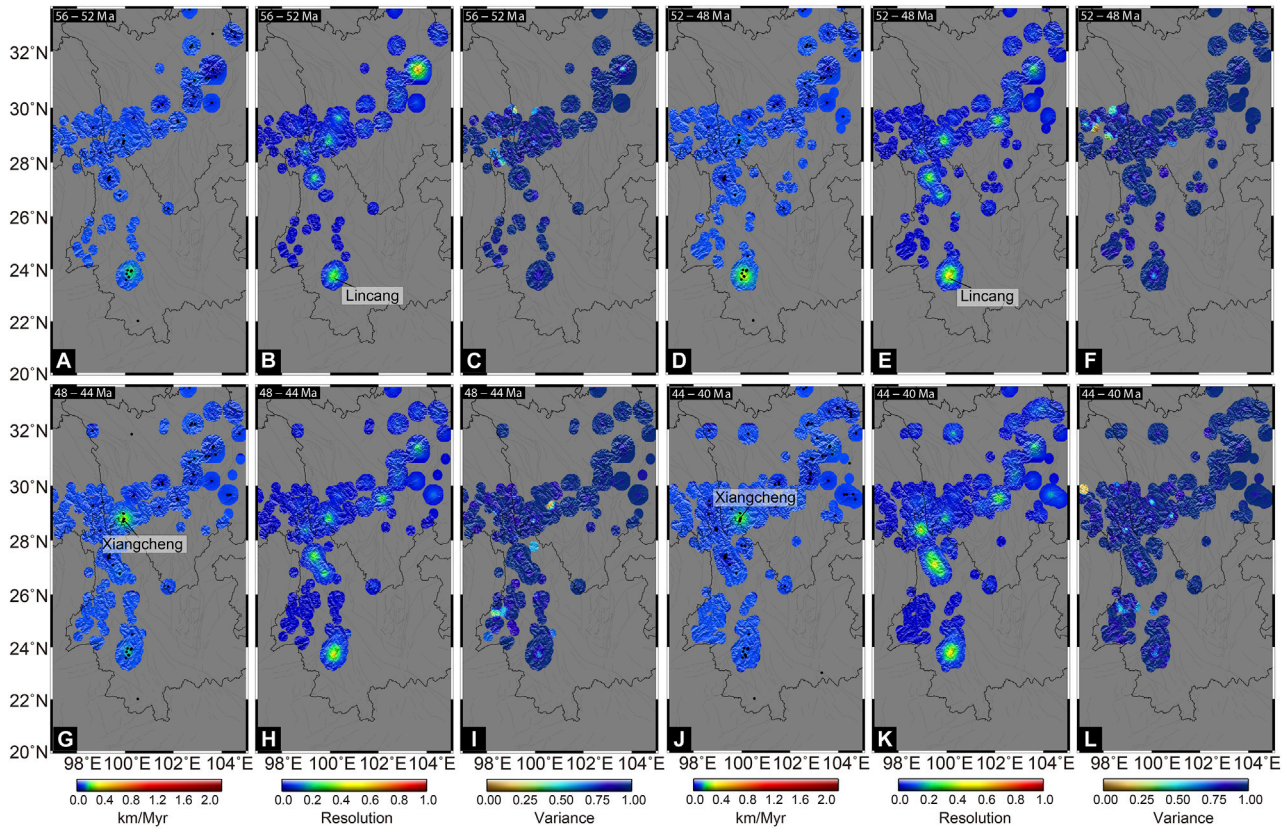

FIGURE 5
Results of the inversion during the Early–Late Eocene. **(A)** Exhumation rates, **(B)** Resolution, and **(C)** Variance of 56–52 Ma; **(D)** Exhumation rates, **(E)** Resolution, and **(F)** Variance of 52–48 Ma; **(G)** Exhumation rates, **(H)** Resolution, and **(I)** Variance of 48–44 Ma; **(J)** Exhumation rates, **(K)** Resolution, and **(L)** Variance of 44–40 Ma.

(AFT = 22, AHe = 15, and ZHe = 9) were available; on analyzing the data, four peaks were revealed (Figure 3E): 36–35 Ma (AFT/ZHe), 27–24 Ma (AFT/ZHe), 18–15 Ma (AFT/AHe/ZHe), and 11–6 Ma (AFT/AHe/ZHe). As compared to other terranes/units, the western Yunnan Terrane generated six age peaks. The oldest peak was recorded by the ZFT ages at ~58 Ma, which was followed by the AFT, AHe, and ZHe age clusters at 38 Ma. In addition, four other young peaks were reported, which included 30–24 Ma (AFT/AHe), 13 Ma (AHe/ZHe), 6 Ma (AFT), and 4 Ma (AHe) (Figure 3F).

In summary, the results revealed synchronous exhumation events in the different terranes/units of the SE Tibetan Plateau despite the existence of variable tectonic environments. We, therefore, suggest that the SE Tibetan Plateau might have experienced at least six rapid exhumation events since the Cenozoic, including ~61–58 Ma, 38–35 Ma, 32–23 Ma, 18–13 Ma, 11–6 Ma, and 4–3 Ma.

4.2 Temporal and spatial evolution of exhumation rates since the Cenozoic

4.2.1 Paleocene (64–56 Ma)

During the Paleocene, especially before 60 Ma, the exhumation rate history was poorly constrained, as indicated by a reduced variance close to 1 in most regions (Figures 4A–C). Areas with relatively high resolution (maximum value of 0.65) were reported only in Xiangcheng of the Songpan–Ganzi–Yidun Terrane and Weixi of the western Yunnan Terrane, but the observed exhumation rates were mainly around 0.1 km/Myr (Figure 4A). From 60 to 56 Ma, more and more data are available and widely distributed. This stage of the model (Figures 4D–F), therefore, is better resolved than the previous stage. The highest exhumation rate was mainly observed in the Lincang area, ranging from 0.23 to 0.3 km/Myr. On the contrary, the exhumation rates in Xiangcheng and Weixi were maintained during this period (Figure 4D).

4.2.2 Early–Late Eocene (56–40 Ma)

At this stage, such low exhumation rates prevailed in most parts of the SE Tibetan Plateau during the whole modeling time period apart from two areas (Xiangcheng and Lincang), in which relatively higher exhumation rates were reported (Figure 5). The rate of exhumation in Lincang has remained at around 0.3 km/Myr between 56 Ma and 48 Ma, in accordance with the Paleocene. On the contrary, a high exhumation rate was reported in Xiangcheng (0.32 km/Myr) at 48–40 Ma.

4.2.3 Late Eocene–Early Oligocene (40–32 Ma)

The exhumation rates in the entire SE Tibetan Plateau remained relatively stable between 40 Ma and 36 Ma (Figures 6A–C). After

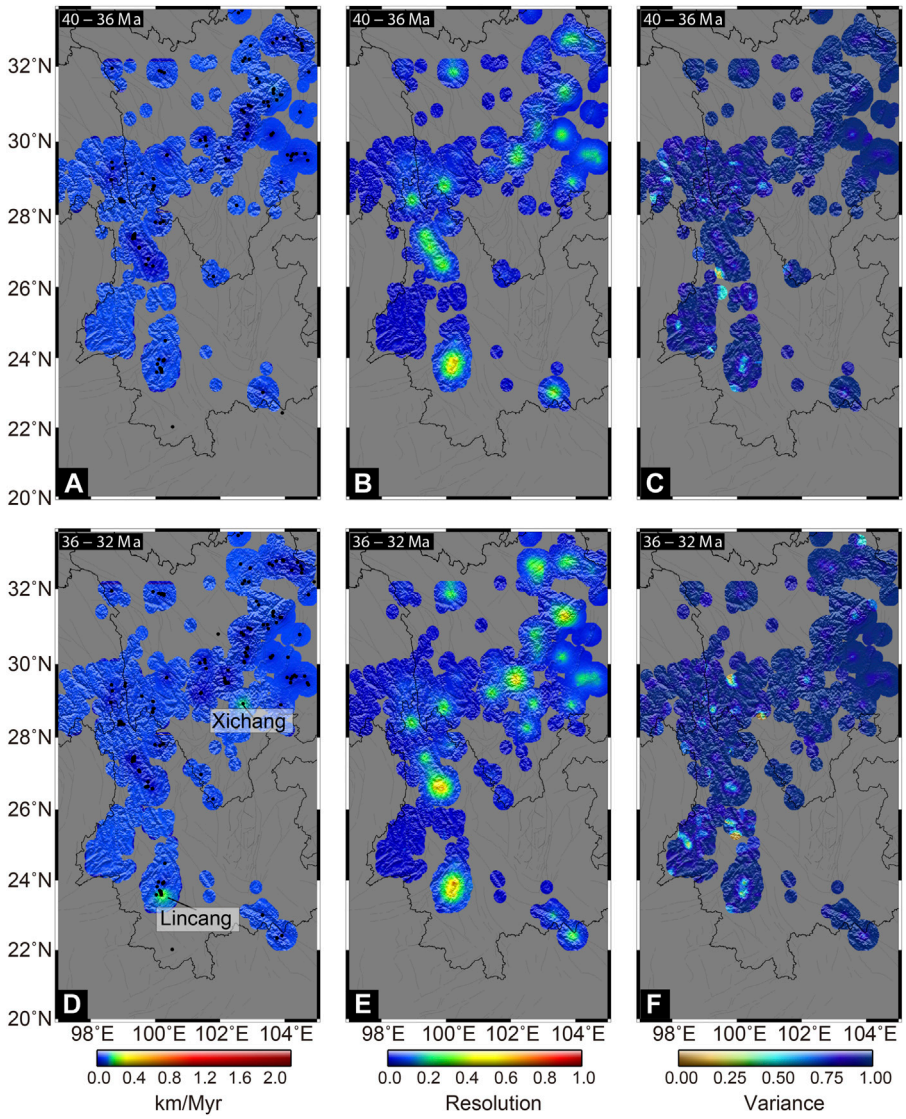

FIGURE 6
Results of the inversion between the Late Eocene and Early Oligocene. **(A)** Exhumation rates, **(B)** Resolution, and **(C)** Variance of 40–36 Ma; **(D)** Exhumation rates, **(E)** Resolution, and **(F)** Variance of 36–32 Ma.

36 Ma, a rapidly increasing trend was observed across the Xichang Basin and Lincang, with values reaching up to 0.18 km/Myr and 0.27 km/Myr, respectively (Figures 6D–F). These inversion results reveal that these areas experienced rapid cooling, which is consistent with the KDE results (Figures 3E, F).

4.2.4 Oligocene (32–24 Ma)

After 32 Ma, the Longmen Shan fault began to undergo significantly differential exhumation (Figure 7). The exhumation rates in the middle and southern segments increased rapidly from less than 0.1 km/Myr to 0.2 km/Myr (southern) to 0.35 km/Myr (middle). On the contrary, the northern segment still exhibited a lower exhumation rate, which is consistent with previous findings (Li et al., 2012; Tan et al., 2014). Additionally, a significant increase in the exhumation rate, that is, 0.25 km/Myr and 0.18 km/Myr, was reported in the Jianchuan Basin and Lincang regions, respectively. Furthermore, the Jianchuan Basin underwent rapid exhumation until the Early Miocene. At the interval of 28–24 Ma, increased exhumation was observed in Gongga Mountain in the Songpan–Ganzi–Yidun Terrane with a maximum rate of 0.44 km/Myr, followed by the Jiulong area (Yunongxi fault) on the western side which experienced an exhumation rate of 0.31 km/Myr.

4.2.5 Miocene (24–8 Ma)

We discovered that during the Early Miocene (24–20 Ma), the middle segment of the Longmen Shan fault became reactive (Wang E. et al., 2012; Tan et al., 2014), experiencing exhumation rates up to 0.46 km/Myr or higher (Figures 8A–C). In the southern segment, the exhumation rate increased to 0.78 km/Myr in Gongga Mountain and Jiulong. At the same intervals, a significant increase in exhumation was observed along Lincang and northern parts of the Ailao Shan–Red River shear zone (up to ~0.3 km/Myr), while the exhumation rate remains

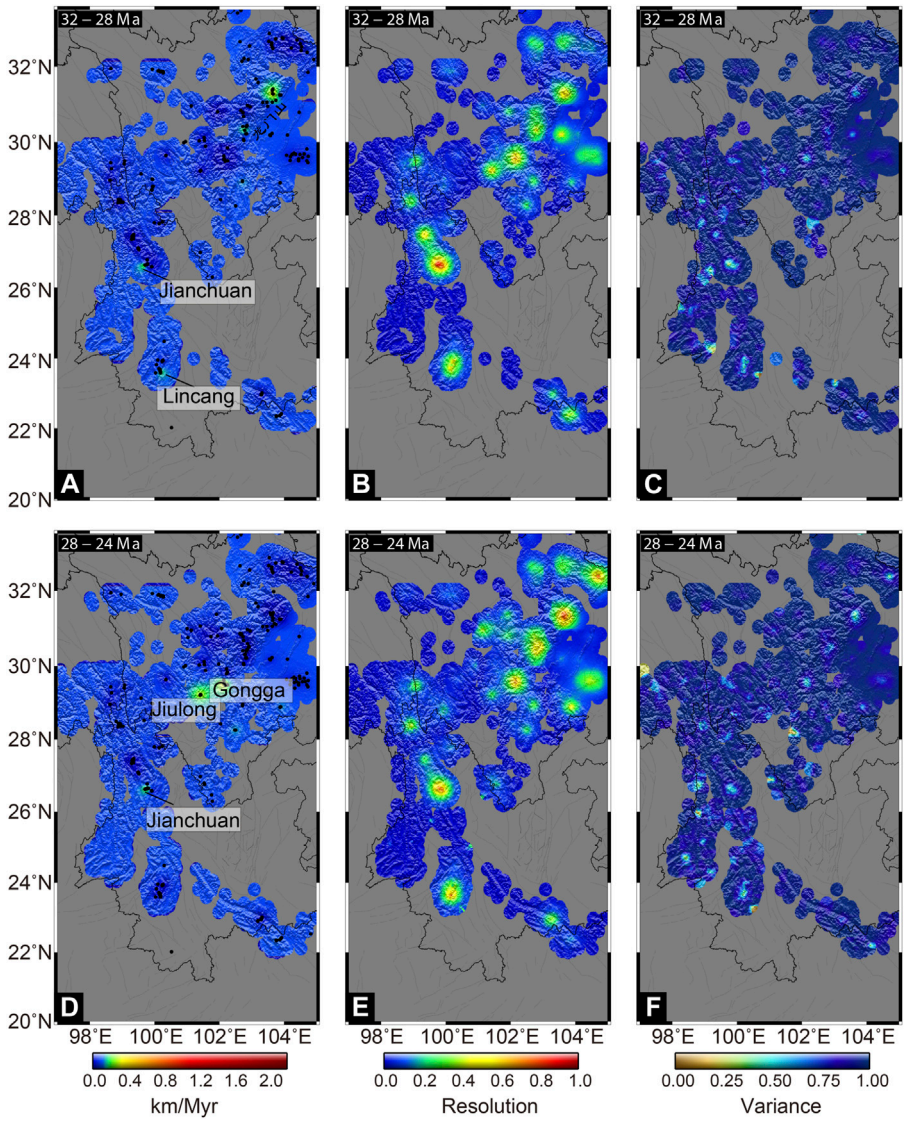

FIGURE 7
Results of the inversion during the Oligocene. **(A)** Exhumation rates, **(B)** Resolution, and **(C)** Variance of 32–28 Ma; **(D)** Exhumation rates, **(E)** Resolution, and **(F)** Variance of 28–24 Ma.

relatively lower than that experienced by the Longmen Shan fault. From the Early to Middle Miocene, the exhumation rates of the Songpan–Ganzi–Yidun and western Yunnan terranes continued to increase yet were mainly concentrated in the area south of 31°N (Figures 8D–F). Since 16 Ma, exhumation was recorded in most parts of the SE Tibetan Plateau with a better resolution, such as the Gaoligong shear zone, the middle segment of the Longmen Shan fault, and the Xianshui River fault (Figures 8G–L).

4.2.6 Pliocene—present day (8–0 Ma)

After 8 Ma, the locus of rapid exhumation migrated from the Gaoligong–Chongshan shear zone south of 26°N to the north and south sides until 4 Ma (Figures 9A–C). Following that, the whole shear zone experienced a high exhumation rate (i.e., up to 1.6 km/Myr). Similarly, before the Pliocene, rapid exhumation of Songpan–Ganzi–Yidun and Longmen Shan–Sichuan terranes/units mainly occurred between 29°N and 31°N, but later, incidences of rapid exhumation occurred throughout the entire region, and the highest rate of more than 2 km/Myr was reached (Figures 9D–F).

5 Discussion

5.1 Influence of parameter setting on modeled exhumation rates

The results presented in Figures 4–9 represent one solution (M_1) amongst a series of acceptable solutions utilizing various parameters or *a priori* models. However, previous studies have suggested that some factors, such as the geothermal gradient,

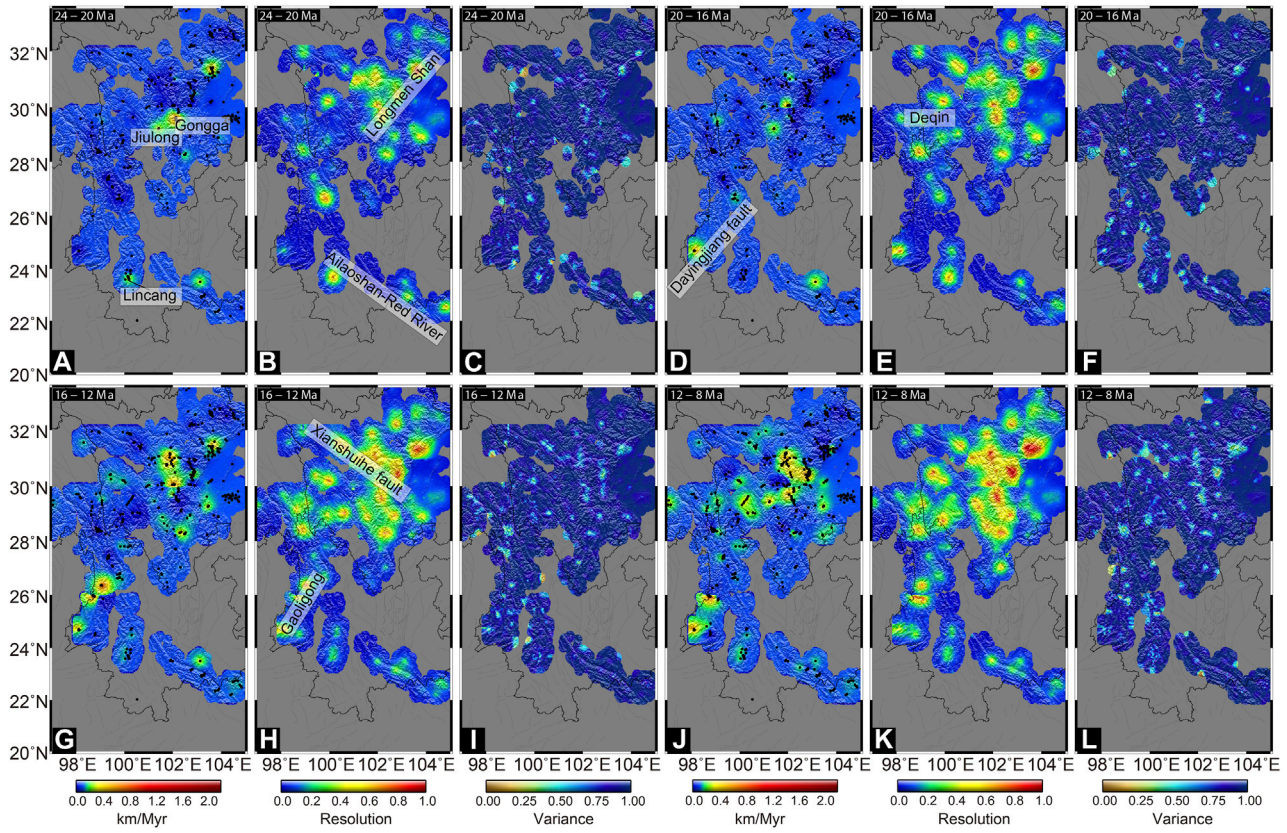

FIGURE 8
Results of the inversion during the Miocene. **(A)** Exhumation rates, **(B)** Resolution, and **(C)** Variance of 24–20 Ma; **(D)** Exhumation rates, **(E)** Resolution, and **(F)** Variance of 20–16 Ma; **(G)** Exhumation rates, **(H)** Resolution, and **(I)** Variance of 16–12 Ma; **(J)** Exhumation rates, **(K)** Resolution, and **(L)** Variance of 12–8 Ma.

prior exhumation rate, time interval, and data search radius (correlation length), could affect the modeled results (Fox et al., 2014; Ballato et al., 2015; Yang et al., 2016; Siravo et al., 2019; Stalder et al., 2020). To verify the reliability of our inversion, we performed a sensitivity study to explore the aforementioned parameters (Supplementary Tables S1, S2; Supplementary Figures S1–S4).

Figures 10, 11; Supplementary Materials indicate that different parameters may affect the inversion results. First, an increase in a geothermal gradient from 25°C/km to 30°C/km may lead to a lower exhumation rate because heat is more efficiently advected to the surface, and thus, the closure depths are shallower (Figures 10A, D). Second, the variations in the *a priori* exhumation rate can potentially be relevant. In case of inadequate data resolution (fewer data; Figures 11A, B), these data are not sufficient to restrict the exhumation rate well within the function interval (sampling interval) during the calculation. Consequently, the model solution is particularly sensitive to the *a priori* model (Figures 10A, B). In this case, our model values do not deviate from the *a priori* parameter. In other words, at the initial stage of calculation, when the prior exhumation rate was large, the calculated result was larger than the small one. Alternatively, as the resolution of the data increases, there may be an artifact of a sharp increase or decrease in the exhumation rate (Fox et al., 2014; Willett et al., 2020). In addition, the time interval and the correlation length of the samples also affected the modeled results. Smaller time intervals and shorter sample correlation lengths reduce the amount of data available to calculate exhumation rates in a given area, increasing the value of data variance and reducing resolution. On the contrary, when both of them increase, restriction of exhumation rates in the calculated area was facilitated (Fox et al., 2016; Stalder et al., 2020; Figures 10A, C).

However, the aforementioned results only have a strong influence on areas with lower resolution (Figures 10A–E, Figures 11A–E) but are weaker for the higher-resolution areas (Figures 10F–J, Figures 11F–J). Furthermore, previous studies have shown that *a priori* values have little impact on the final simulation results (Fox et al., 2014; Willett et al., 2020). To ensure reliability of the results, we only analyzed the areas having more than 0.25 resolution (Herman et al., 2013).

Similarly, we have illustrated the frequency of the difference between predicted and measured ages (misfit) for the different models through a histogram (Figure 12). Notably, the results pertaining to different parameter simulations did not vary obviously (Figure 12), and the differences mainly ranged between −5 Ma and 5 Ma. We statistically analyzed the misfit values of the various models independently, to examine the impact of each parameter on the results pertaining to age prediction, and the outcomes; the results are illustrated in Supplementary Table S2. M_1, which considers the data dispersion and practical needs, was ultimately selected as the optimal model for

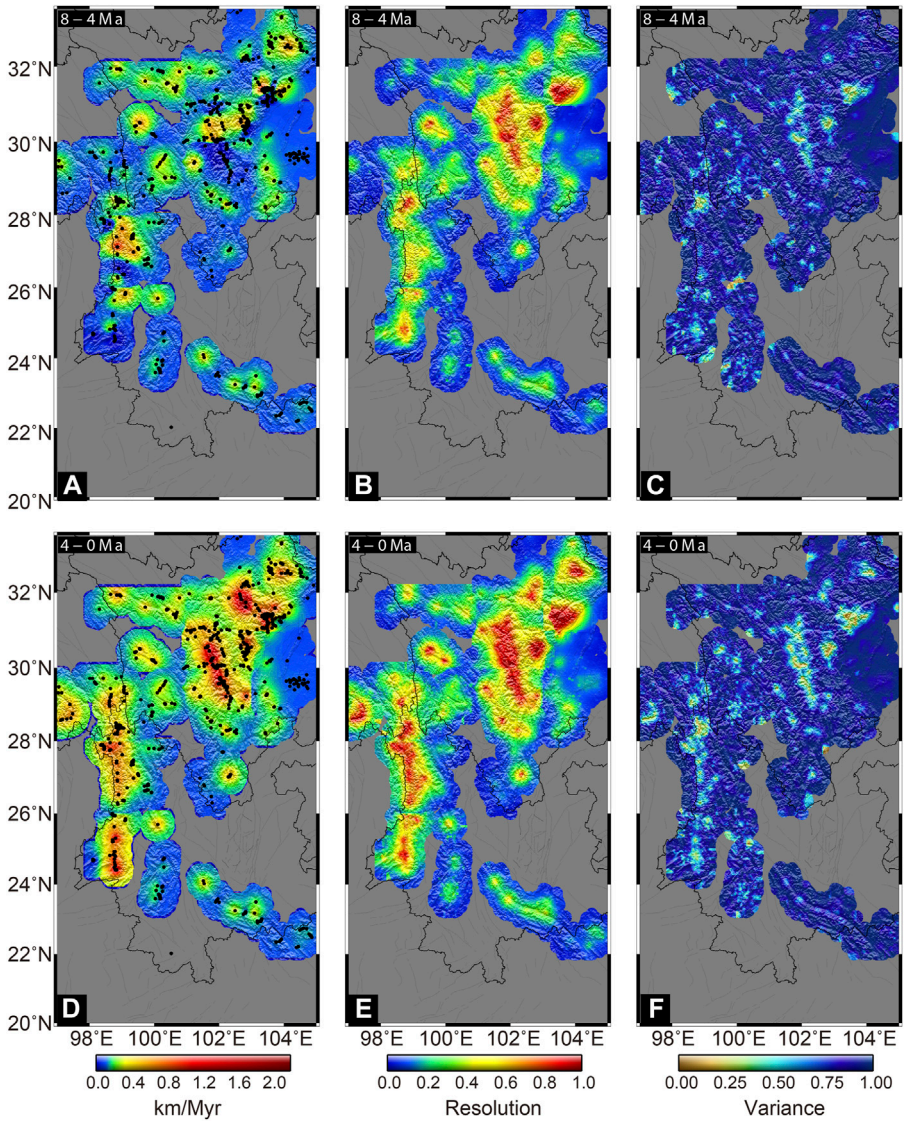

FIGURE 9
Results of the inversion since the Pliocene. **(A)** Exhumation rates, **(B)** Resolution, and **(C)** Variance of 8–4 Ma; **(D)** Exhumation rates, **(E)** Resolution, and **(F)** Variance of 4–0 Ma.

analysis, even though the findings pertaining to other parameters were slightly different.

5.2 The dynamic mechanism for the Cenozoic exhumation history

Our findings suggest that the rapid Cenozoic cooling episode initially occurred during the Paleocene (Figure 3). This event was recorded not only in the SE Tibetan Plateau but also in the central, northern, and eastern parts of the plateau (Hetzel et al., 2011; Rohrmann et al., 2012; Dai et al., 2013; Haider et al., 2013; Jian et al., 2018). Such a synchronous and widespread exhumation suggested a regional event at this stage: crustal shortening due to large-scale tectonic activity with the beginning of the collision between the Indian and Eurasian continents (England and Searle, 1986; Murphy et al., 1997; Kapp et al., 2005; Kapp et al., 2007). Although the onset of the India–Eurasia collision remains controversial, the prevailing viewpoint suggests 65–55 Ma (Wang et al., 2014), which overlaps with the Paleocene rapid exhumation event. During this period, the compressive stress trending N–S was promptly transmitted to the northern margin of the plateau, activating the former and deep faults, leading to thrust faulting and folding, and characterization of the orogen, as illustrated in the low-temperature thermochronology data (e.g., He et al., 2017; Liu and Cai, 2022). These views support the immediate response model for growth of the Tibetan Plateau (e.g., Dayem et al., 2009) but contradict the models that support diachronous progressive growth from south to north (e.g., Tapponnier et al., 2001).

By the Early–Middle Eocene, our KDE results could not depict an age peak, but higher exhumation rates were observed in the local regions (i.e., Lincang and Xiangcheng). Furthermore, such a phase of

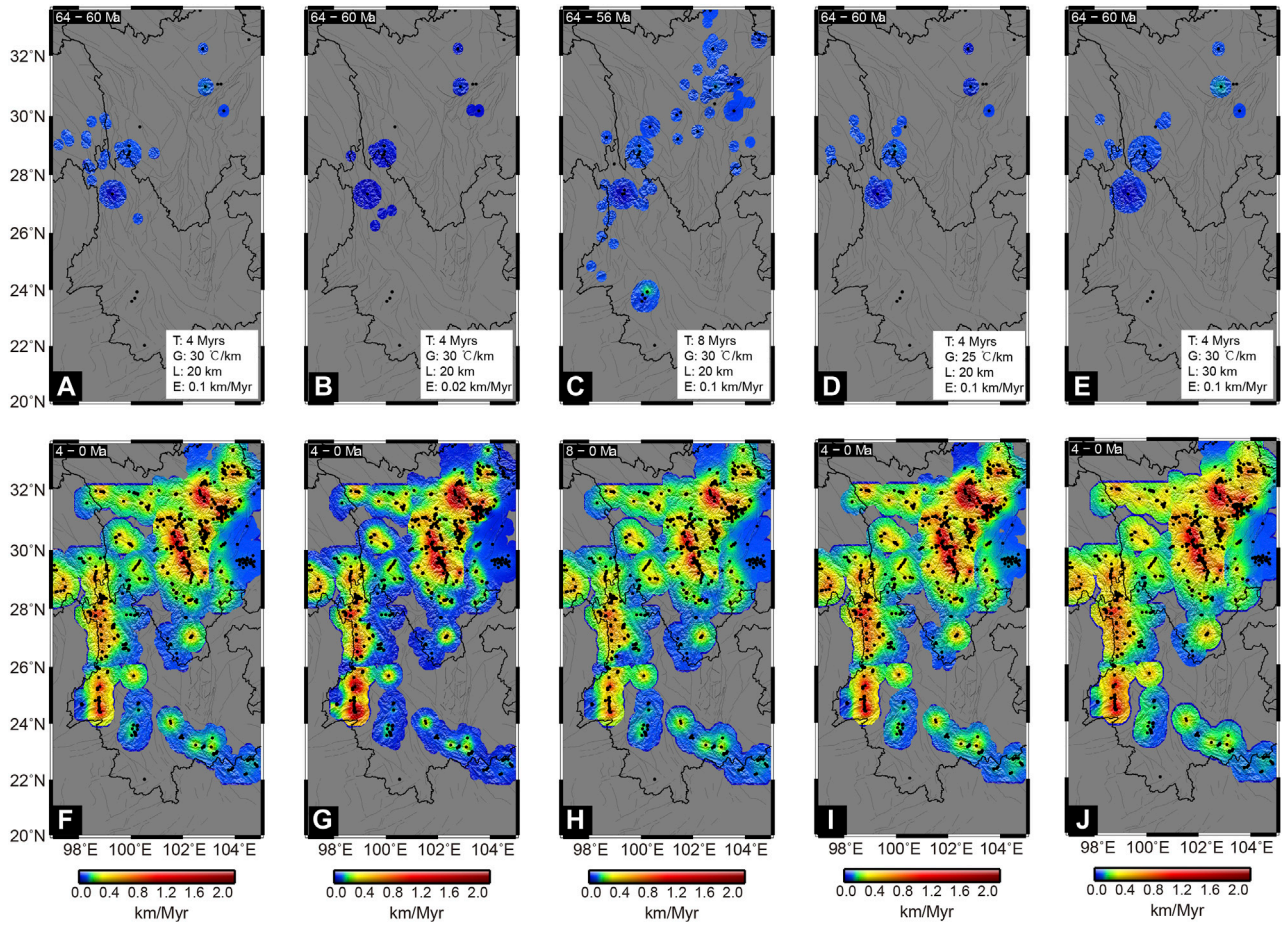

FIGURE 10
Influence of model parameters on the exhumation rates of **(A–E)** initial and **(F–J)** recent timestep (parameter symbols are the same as in Supplementary Tables S1, S2, the same as the following figure).

exhumation was also reported at Weixi and Deqin (Figure 13A), with a rapid exhumation rate of ~0.1–0.3 km/Myr, as revealed by AFT and AHe data (Liu-Zeng et al., 2018b). It is worth noting that Ou et al. (2020) recalculated a rate of 0.04–0.06 km/Myr, at this stage, using 3D thermo-kinematic modeling near Deqin, and their findings are consistent with our findings obtained from inversions (Figure 5; Supplementary Materials). Nevertheless, the report of the Early–Middle Eocene phase of exhumation remains limited and suggests that it is probably a local signal (Zhang et al., 2022).

During the Late Eocene–Early Oligocene, the linear inversion results revealed that the Xichang Basin and Lincang generated enhanced exhumation rates (Figure 6), which were confirmed by previous results and our KDE results (Figures 3, 13A). We concluded that a tectonic shortening mechanism may explain why the aforementioned two regions experienced rapid uplift during this phase (Deng et al., 2018; Liu et al., 2021). At this stage, the Indian plate continued to move northward, and under the influence of oblique compressional collision, strong tectonic deformation began in the SE Tibetan Plateau, subsequently leading to development of numerous thrust-nappe tectonic belts and strike-slip shear zones, accompanied by a series of contemporaneous igneous rocks (Wang and Burchfiel, 1997; Tapponnier et al., 2001). These phenomena have been observed in Lincang and Xichang Basins. For example, the low-temperature thermochronological data identified that the Xichang Basin underwent protracted cooling at 40–20 Ma with a rate of 0.1–0.3 km/Myr (Deng et al., 2018), and the findings are consistent with our results (Figures 6D–F). Meanwhile, they also recovered the stratigraphy from the Late Triassic in and around the Xichang Basin by balanced cross-sections and hypothesized some shortening of ~20–30 km occurred in the east–west direction. Furthermore, there are only two unconformities among the upper Triassic and pre-Late Triassic sequences (T_3/P), Neogene, and its underlying strata (N_2/E_1) in the Xichang Basin (Deng et al., 2018). Considering the aforementioned points, we speculated that the shortening should be explained in terms of Cenozoic shortening, rather than an average shortening since the Late Triassic. Meanwhile, the intermontane Lanping–Simao Basin was folded, closed, and converted into a mountain, with simultaneous molasse sediment signals in the front of the mountains between the Late Eocene and Oligocene (He et al., 1996; Wang and Burchfiel, 1997). In addition, the abundant Eocene–Oligocene thrust-nappe tectonic belts were developed in the interior and margin of the Lincang granite batholith, which was composed of several thrust or oblique faults with right strike-slip characteristics (Li, 1994; Wu, 1994; Liu et al., 1998). Amidst such thrust-nappe activities, the Lincang granite

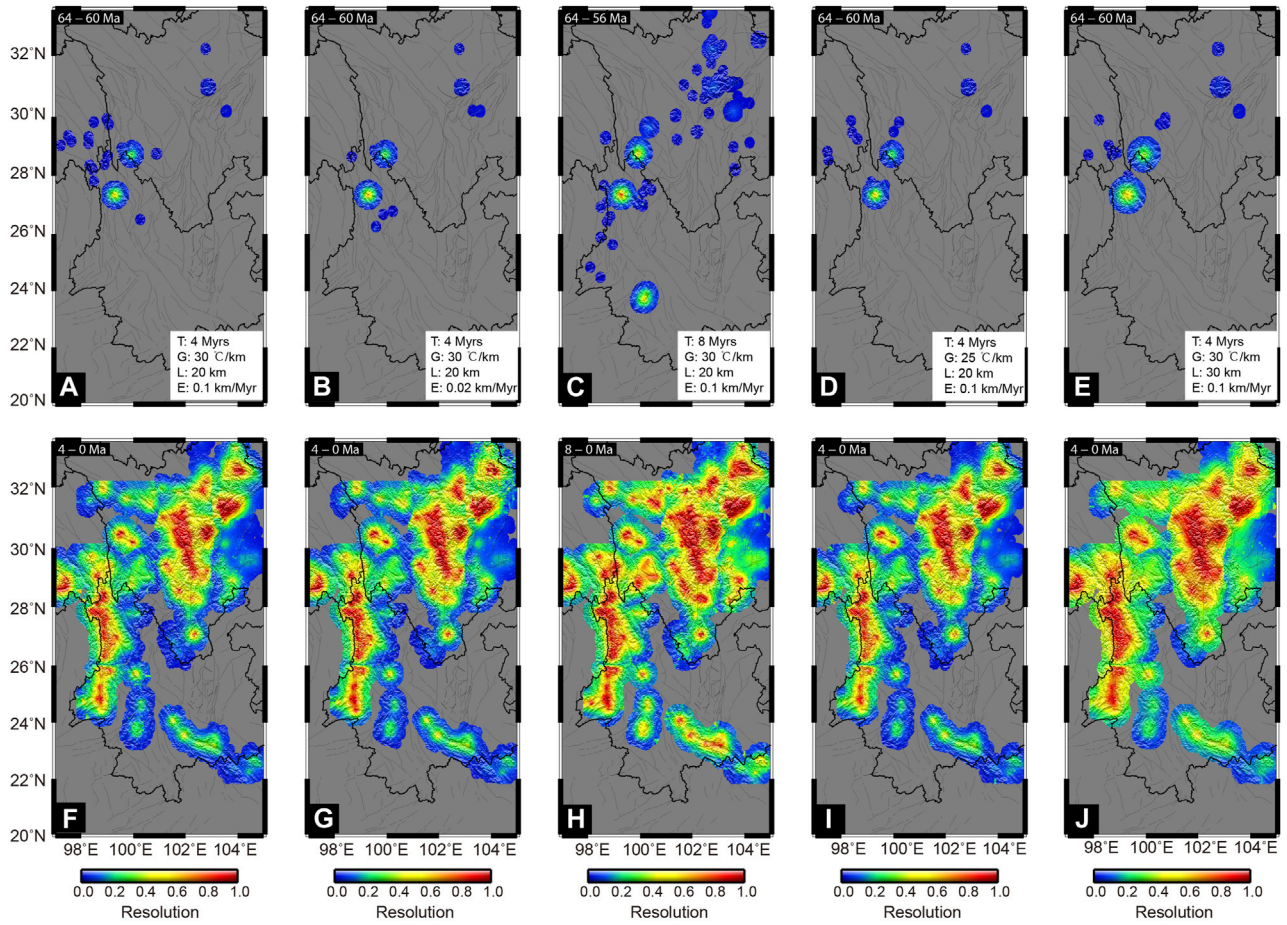

FIGURE 11
Resolution of the inversion results of **(A–E)** initial and **(F–J)** recent timesteps shown in Figure 10.

batholith was uplifted and exhumed at a large scale (Shi et al., 2006). Similarly, upper Eocene to Oligocene detrital strata overlying the older deformed strata underwent regional unconformity in the Simao and Baoshan/Lincang blocks of the SE Tibetan Plateau, indicating the beginning of shortening deformation (Wang and Burchfiel, 1997).

The Oligocene cooling phase is coeval with those reported around the SE Tibetan Plateau, suggestive of enhanced exhumation on a regional scale (Figure 3). At the northeastern terminus of the Nantinghe fault, this Oligocene cooling was determined by thermal modeling based on the AHe age (Wang et al., 2019; Sample LC03-1), which may result due to tectonic transtension/transpression toward the northeastern termination. Cao et al. (2020) revealed rapid exhumation of 2.3–2.5 km at ~28–20 Ma (Figure 13A) in the north of the Jianchuan Basin. They inferred the current relief of the SE Tibetan Plateau can be triggered by the Yulong thrust belt, while the possibility of crustal thickening and increase in elevation before the Oligocene or Early Cenozoic collision of India–Asia cannot be ignored. In contrast, Shen et al. (2016) recognized a phase of exhumation in the Jianchuan Basin between 30 and 20 Ma with a rate range of ~0.10–0.18 km/Myr (Figure 13A), resulting from the transpressional deformation in the SE Tibetan Plateau.

The Early Oligocene rapid exhumation and uplift of the Lincang granite batholith overlay with the dextral/sinistral strike-slip movement, such as Gaoligong, Chongshan, and Ailao Shan–Red River shear zones, even though the initial timing of their activities is debatable (Leloup et al., 1993; Leloup et al., 2001; Gilley et al., 2003; Akciz et al., 2008). Since the Oligocene, the rocks located in these shear zones underwent shortening, extruding toward the southeast, and differential clockwise rotation, consistent with the current crustal motion derived by GPS (Pan and Shen, 2017). Such kinematic properties indicate that they are significant to absorb hundreds of kilometers of displacement of the SE Tibetan Plateau (Wang and Burchfiel, 1997; Yin and Harrison, 2000; Gilley et al., 2003; Akciz et al., 2008).

We observe that since the Middle Miocene, the entire SE Tibetan Plateau exhibited significantly accelerated exhumation, particularly in the Gaoligong shear zone, the middle segment of the Longmen Shan fault, and the Xianshui River fault (Figure 8). Ge et al. (2020) used thermal history inversion to derive a rapid exhumation rate of 0.4–0.6 km/Myr at this stage, and our simulation results align with the finding (Figure 8). They suggested that such an enhanced exhumation phase should be attributed to the tectonics, combined with previous $^{40}Ar/^{39}Ar$ and U-Pb dating (Akciz et al., 2008; Lin et al., 2009). However, we concluded that this phase of rapid cooling was caused by intensified monsoon precipitation (Nie et al., 2018; Liu et al., 2021). At 17–14 Ma, the globe was in a period

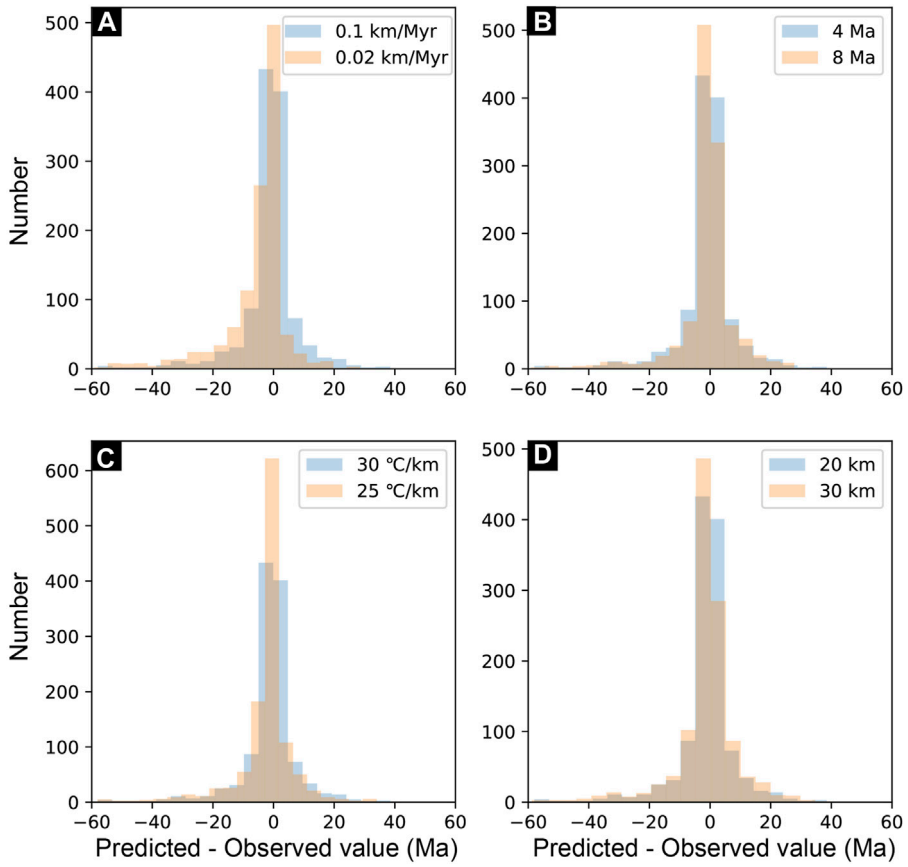

FIGURE 12
Histogram of the difference between model-predicted and observed ages. **(A)** Prior exhumation rate; **(B)** Time interval; **(C)** Initial geothermal gradient; **(D)** Correlation length.

of Middle Miocene Climate Optimum, and increased CO_2 levels and warm climate were the main factors contributing to enhanced precipitation from the Asian summer monsoon during this period (Licht et al., 2014; Ji et al., 2018). Enhanced precipitation will potentially increase the power of river incision and trigger fault activity, which itself can intensify incision by increasing relief (Eroğlu et al., 2013; Wang et al., 2019). This hypothesis has been clarified by Ren X. et al. (2020). For the Xianshui River fault, previous work has dated U–Pb, mica K–Ar, and AFT to indicate that it initiated to undergo sinistral strike-slip movement at ~15–13 Ma, suggestive of the onset of compression toward the western Sichuan and South China Block (Roger et al., 1995; Wang et al., 2009).

In the Late Miocene, the exhumation rates increased throughout the SE Tibetan Plateau, as compared to the previous phase, particularly in areas lying on the tectonic boundary areas (Figure 9). In addition, the analysis in Figure 3 shows that the entire SE Tibetan Plateau is in a phase of rapid exhumation, which was more widespread than that in the Middle Miocene. Similarly, the widespread rapid exhumation events coincide with the record of intense summer monsoon precipitation in Asia (Ren X. et al., 2020). The increased precipitation events of the Late Miocene may be attributed to an enhanced monsoon driven by tectonic uplift along the NE Tibetan Plateau compared to the enhanced monsoon brought about by global warming in the Miocene (Prell and Kutzbach, 1992; An et al., 2001). Topographic uplift helped in overcoming the effects of a cooler climate and decreased moisture level in the air (Ji et al., 2018) by intensifying the sea–land pressure gradient (An et al., 2001). Therefore, it was hypothesized that the uplift-driven monsoon intensification may lead to the rapid incision of the entire SE Tibetan Plateau. Furthermore, we collected paleoclimatic data for the Late Miocene period in Yunnan, when higher temperature and precipitation occurred as compared to the present era, with an annual mean precipitation of approximately 1,000–1,600 mm, which is indicative of a strong precipitation effect in Yunnan during the Late Miocene (Figures 13B, C). However, the tectonic possibilities cannot be ruled out. For example, in the Gaoligong–Chongshan shear zone, Wang et al. (2019) used apatite and zircon (U-Th)/He to derive two phases of rapid exhumation history in the area since the Late Cenozoic, one of which was prior to 11 Ma (15–11 Ma) and the other at 8–6 Ma (Figure 13A). The earlier one is linked with ductile transpressional shearing. However, the exhumation event at the Dayingjiang fault was caused by the sinistral transtension of a strike-slip fault (Wang et al., 2019). In the farther northern areas of the SE Tibetan Plateau, widespread rapid exhumation events were witnessed during the Late Miocene (Figure 13A), such as in the Longmen Shan (Kirby et al.,

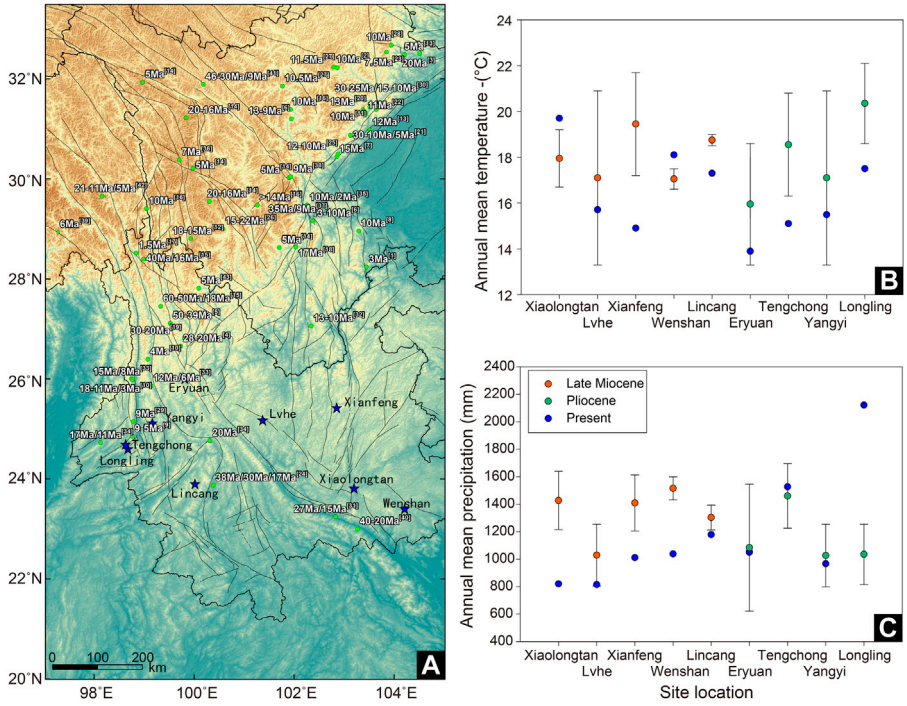

FIGURE 13
(A) Site map with low-temperature thermochronology (green circle), temperature (blue star), and precipitation (blue star) in the SE Tibetan Plateau; **(B)** annual mean temperature distribution; **(C)** annual precipitation distribution. The precipitation data are derived from references (Xu, 2002; Kou et al., 2006; Xu et al., 2008; Xia et al., 2009; Guo, 2011; Jacques et al., 2011; Sun et al., 2011; Xing et al., 2012; Li S.-F. et al., 2015), and the low-temperature thermochronology data are derived from references [(1) = An et al., 2008; (2) = Ansberque et al., 2018; (3) = Arne et al., 1997; (4) = Cao et al., 2019; (5) = Cao et al., 2020; (6) = Clark et al., 2005; (7) = Cook et al., 2013; (8) = Deng et al., 2014; (9) = Eroğlu et al., 2013; (10) = Ge et al., 2020; (11) = Godard et al., 2009; (12) = Gourbet et al., 2019; (13) = Kirby et al., 2002; (14) = Lai et al., 2007; (15) = Liu-Zeng et al., 2018b; (16) = Ouimet et al., 2010; (17) = Replumaz et al., 2020; (18) = Wang S. et al., 2012; (19) = Shen et al., 2016; (20) = Shen et al., 2019; (21) = Tan et al., 2014; (22) = Tan et al., 2017; (23) = Tan et al., 2019; (24) = Liu et al., 2021; (25) = Tian et al., 2013; (26) = Tian et al., 2014; (27) = Tian et al., 2015; (28) = Tian et al., 2018; (29) = Wang et al., 2008; (30) = Wang E. et al., 2012; (31) = Wang et al., 2016; (32) = Wang et al., 2017; (33) = Wang et al., 2018; (34) = Wang et al., 2019; (35) = Yang R. et al., 2020; (36) = Zhang et al., 2015; (37) = Zhang et al., 2016; (38) = Zhang et al., 2017; (39) = Lei et al., 2008; (40) = Ren L. et al., 2020; (41) = Wang et al., 2015; (42) = Xiao et al., 2015; (43) = Zou et al., 2014].

2002; Godard et al., 2009), Jiulong (Zhang et al., 2016), Min River (Tian et al., 2015), Min Shan (Tian et al., 2018), Xianshuihe fault (Zhang et al., 2017), Maoergai fault (Ansberque et al., 2018), Dadu River (Clark et al., 2005; Ouimet et al., 2010; Tian et al., 2015), the Daliang Mountains (Deng et al., 2014), and Anning River (Clark et al., 2005). Tian et al. (2013, 2015) suggested that time synchronization between the large-scale exhumation and rock and surface uplift in the Late Miocene was closely associated with crustal shortening rather than climatic effect, highlighting the role of crustal shortening in forming the enhanced erosion and high elevation of the plateau margin. In contrast, Clark et al. (2005) inferred that this synchronous event supported the tectonic (lower crustal flow)-climate (Asian summer monsoon) models.

During the Pliocene, despite the absence of significant fault activities in the Gaoligong–Chongshan shear zone, a rapid cooling event occurred in the region, which is thought to have been forced by climate-driven rapid incision of rivers or the injection of lower crustal flows (Wang et al., 2018; Ge et al., 2020). In contrast, Eroğlu et al. (2013) suggested that this rapid exhumation was triggered by crustal root delamination and the opening of the Andaman Sea. Additionally, in the Deqin–Zhongdian area, Xiao et al. (2015) and Zou et al. (2014) used AHe and AFT dating to derive a rapid cooling event since the Pliocene (5 Ma), and the calculated exhumation rates lay in the range of 0.3–0.4 km/Myr; our simulation results are consistent with the findings (Figure 9). However, there is an obvious difference in the explanation provided. Xiao et al. (2015) attributed the event to intense erosion due to strong precipitation from the Indian monsoon and the onset of the global glacial period. In contrast, Zou et al. (2014) revealed that it was caused by tectonic uplift, but no explanatory reason has been provided. In the Longmen Shan fault, the eastern margin of the Tibetan Plateau underwent a phase of eastward expansion due to strike-slip fault deformations and thrusting, and upper crustal deformation resulted in the formation of the Ganzi–Litang margin in the Miocene and continued to move toward the Longmen Shan fault around 5 Ma (Lai et al., 2007). The Xianshuihe fault, which intersects the Longmen Shan fault, played an important role in the tectonic evolution of the Tibetan Plateau. As discussed previously, the Xianshuihe fault began to undergo sinistral strike-slip movement at 15–13 Ma and was reactivated at 5 Ma, thereby cutting through the Longmen Shan fault and extending southward into the Xiaojiang fault zone (Roger et al., 1995; Wang et al., 2009).

Since 4 Ma, exhumation rates have experienced a general increase across the SE Tibetan Plateau (Figures 9D–F). An et al. (2008) suggested that the event was controlled by the tectonics, while other authors suggested that climate was the main driving force that controlled the river incision but did not exclude a tectonic role. Herman et al. (2013)

used the Glide software application to invert the global cooling event by collecting nearly 18,000 low-temperature thermochronology data from different regions of the world. They found that erosion rates increased in all regions from 6 Ma, with a particularly noticeable increase from 2 Ma, and suggested that glaciation played a crucial role in this global increase in erosion rates. In the Qaidam Basin at the NE Tibetan Plateau, Ren X. et al. (2020) synthesized previous studies and demonstrated that a total of two intense precipitation events occurred at 4–2.7 Ma and 0.4 Ma. They illustrated that the former event was attributed to the further uplift of the Tibetan Plateau or closure of the Panama Seaway, whereas the latter may reflect a weak El Niño-like phenomenon related to high zonal sea surface temperature gradients. Therefore, we argue that climate forcing can play a key role in this cooling episode, along with minor tectonism.

6 Conclusion

(1) At least six rapid exhumation events occurred since the Cenozoic across the SE Tibetan Plateau, including ~61–58 Ma, 38–35 Ma, 32–23 Ma, 18–13 Ma, 11–6 Ma, and 4–3 Ma.
(2) From the Paleocene to Oligocene, the exhumation rates were relatively low throughout the SE Tibetan Plateau, with rapid exhumation occurring in Xiangcheng of the Songpan–Ganzi–Yidun Terrane and Lincang of the western Yunnan Terrane. We infer that the rapid cooling episodes during this period may be attributed to the oblique extrusion and continuous convergence of the Indian and Eurasian plates.
(3) During the Early Miocene to Middle Miocene, although the areas of rapid exhumation gradually expanded and the exhumation rates increased significantly, they were mainly distributed in the area south of 31°N. From the Late Miocene until the present, the entire SE Tibetan Plateau underwent a phase of rapid exhumation, especially in the Xianshuihe fault, the Longmen Shan–Sichuan Basin, and the Gaoligong–Chongshan shear zone. Since the Miocene, strong precipitation from the Asian summer monsoon and the onset of the global glacial period have had an impact on the exhumation rates in the SE Tibetan Plateau. In addition, tectonic activities have also played a non-negligible role in shaping the local landscape.

Data availability statement

The original contributions presented in the study are included in the article/Supplementary Material; further inquiries can be directed to the corresponding author.

Author contributions

Conceptualization: FL and MW; methodology: FL; software: FL; formal analysis: FL and MW; data curation: FL; writing—original draft preparation: FL; writing—review and editing: MW and HL; visualization: FL and RN. All authors contributed to the article and approved the submitted version.

Funding

This research was jointly funded by the Second Tibetan Plateau Scientific Expedition (grant number 2019QZKK0704) and the Horizontal Foundation of the Qilu Normal University (grant number 2021HX002).

Acknowledgments

The authors thank two reviewers for their constructive and helpful comments to improve this manuscript and Associate Professor Liang Zhang for editorial handling. They are very grateful to Dr. Herman and Fox for providing the opening source code (Glide). Most of the figures were drawn using free software GMT developed by Prof. Wessel. They would like to thank KetengEdit (www.ketengedit.com) for linguistic assistance during the preparation of this manuscript.

Conflict of interest

The authors declare that the research was conducted in the absence of any commercial or financial relationships that could be construed as a potential conflict of interest.

Publisher's note

Supplementary material

The Supplementary Material for this article can be found online at: https://www.frontiersin.org/articles/10.3389/feart.2023.1164733/full#supplementary-material

References

Akciz, S., Burchfiel, B. C., Crowley, J. L., Yin, J., and Chen, L. (2008). Geometry, kinematics, and regional significance of the Chong Shan shear zone, eastern himalayan syntaxis, yunnan, China. *Geosphere* 4, 292. doi:10.1130/GES00111.1

An, Y., Han, Z., and Wan, J. (2008). Fission track dating of the Cenozoic uplift in Mabian area, southern Sichuan Province, China. *Sci. China Ser. Earth Sci.* 51, 1238–1247. doi:10.1007/s11430-008-0105-5

An, Z., Kutzbach, J. E., Prell, W. L., and Porter, S. C. (2001). Evolution of Asian monsoons and phased uplift of the Himalaya-Tibetan plateau since Late Miocene times. *Nature* 411, 62–66. doi:10.1038/35075035

Ansberque, C., Godard, V., Olivetti, V., Bellier, O., de Sigoyer, J., Bernet, M., et al. (2018). Differential exhumation across the longriba fault system: Implications for the eastern Tibetan plateau. *Tectonics* 37, 663–679. doi:10.1002/2017tc004816

Arne, D., Worley, B., Wilson, C., She, F. C., Foster, D., Zhi, L. L., et al. (1997). Differential exhumation in response to episodic thrusting along the eastern margin of the Tibetan Plateau. *Tectonophysics* 280, 239–256. doi:10.1016/S0040-1951(97)00040-1

Ballato, P., Landgraf, A., Schildgen, T. F., Stockli, D. F., Fox, M., Ghassemi, M. R., et al. (2015). The growth of a mountain belt forced by base-level fall: Tectonics and surface processes during the evolution of the Alborz Mountains, N Iran. *Earth Planet. Sci. Lett.* 425, 204–218. doi:10.1016/j.epsl.2015.05.051

Batt, G. E., and Braun, J. (1997). On the thermomechanical evolution of compressional orogens. *Geophys. J. Int.* 128, 364–382. doi:10.1111/j.1365-246X.1997.tb01561.x

Braun, J., van der Beek, P., Valla, P., Robert, X., Herman, F., Glotzbach, C., et al. (2012). Quantifying rates of landscape evolution and tectonic processes by thermochronology and numerical modeling of crustal heat transport using PECUBE. *Tectonophysics* 524 (525), 1–28. doi:10.1016/j.tecto.2011.12.035

Burchfiel, B. C., and Chen, Z. (2012). *Tectonics of the southeastern Tibetan Plateau and its adjacent Foreland*. doi:10.1130/MEM210

Cao, K., Leloup, P. H., Wang, G., Liu, W., Mahéo, G., Shen, T., et al. (2020). Thrusting, exhumation, and basin fill on the Western margin of the South China block during the India-Asia collision. *GSA Bull.* 133, 74–90. doi:10.1130/b35349.1

Cao, K., Tian, Y., van der Beek, P., Wang, G., Shen, T., Reiners, P., et al. (2022). Southwestward growth of plateau surfaces in eastern Tibet. *Earth-Sci. Rev.* 232, 104160. doi:10.1016/j.earscirev.2022.104160

Cao, K., Wang, G., Leloup, P. H., Mahéo, G., Xu, Y., van der Beek, P. A., et al. (2019). Oligocene-early Miocene topographic relief generation of southeastern Tibet triggered by thrusting. *Tectonics* 38, 374–391. doi:10.1029/2017tc004832

Clark, M. K., House, M. A., Royden, L. H., Whipple, K. X., Burchfiel, B. C., Zhang, X., et al. (2005). Late cenozoic uplift of southeastern Tibet. *Geology* 33, 525. doi:10.1130/g21265.1

Clark, M. K., and Royden, L. H. (2000). Topographic ooze: Building the eastern margin of Tibet by lower crustal flow. *Geology* 28, 703–706. doi:10.1130/0091-7613(2000)028<0703:tobtem>2.3.co;2

Clark, M. K., Schoenbohm, L. M., Royden, L. H., Whipple, K. X., Burchfiel, B. C., Zhang, X., et al. (2004). Surface uplift, tectonics, and erosion of eastern Tibet from large-scale drainage patterns. *Tectonics* 23. doi:10.1029/2002TC001402

Coleman, M., and Hodges, K. (1995). Evidence for Tibetan plateau uplift before 14 Myr ago from a new minimum age for east-west extension. *Nature* 374, 49–52. doi:10.1038/374049a0

Cook, K. L., Royden, L. H., Burchfiel, B. C., Lee, Y. H., and Tan, X. (2013). Constraints on Cenozoic tectonics in the southwestern Longmen Shan from low-temperature thermochronology. *Lithosphere* 5, 393–406. doi:10.1130/L263.1

Dai, J., Wang, C., Hourigan, J., Li, Z., and Zhuang, G. (2013). Exhumation history of the gangdese batholith, southern Tibetan plateau: Evidence from apatite and zircon (U-Th)/He thermochronology. *J. Geol.* 121, 155–172. doi:10.1086/669250

Dayem, K. E., Molnar, P., Clark, M. K., and Houseman, G. A. (2009). Far-field lithospheric deformation in Tibet during continental collision. *Tectonics* 28. doi:10.1029/2008TC002344

Deng, B., Liu, S., Enkelmann, E., Li, Z., Ehlers, T. A., and Jansa, L. (2014). Late Miocene accelerated exhumation of the Daliang mountains, southeastern margin of the Tibetan plateau. *Int. J. Earth Sci.* 104, 1061–1081. doi:10.1007/s00531-014-1129-z

Deng, B., Liu, S., Lei, J., Zhao, G., Rui, H., Li, Z., et al. (2018). Tectonic uplift of the Xichang Basin (SE Tibetan Plateau) revealed by structural geology and thermochronology data. *Basin Res.* 30, 75–96. doi:10.1111/bre.12243

Dewey, J. F. (1988). The tectonic evolution of the Tibetan plateau. *Philos. Trans. R. Soc. Lond. Math. Phys. Eng. Sci.* 327, 379–413. doi:10.1098/rsta.1988.0135

England, P., and Searle, M. (1986). The cretaceous-tertiary deformation of the Lhasa block and its implications for crustal thickening in Tibet. *Tectonics* 5, 1–14. doi:10.1029/TC005i001p00001

Eroğlu, S., Siebel, W., Danišík, M., Pfänder, J. A., and Chen, F. (2013). Multi-system geochronological and isotopic constraints on age and evolution of the Gaoligongshan metamorphic belt and shear zone system in Western Yunnan, China. *J. Asian Earth Sci.* 73, 218–239. doi:10.1016/j.jseaes.2013.03.031

Fielding, E., Isacks, B., Barazangi, M., and Duncan, C. (1994). How flat is Tibet? *Geology* 22, 163–167. doi:10.1130/0091-7613(1994)022<0163:hfit>2.3.co;2

Fox, M., Herman, F., Willett, S. D., and May, D. A. (2014). A linear inversion method to infer exhumation rates in space and time from thermochronometric data. *Earth Surf. Dyn. Discuss.* 2, 47–65. doi:10.5194/esurf-2-47-2014

Fox, M., Herman, F., Willett, S. D., and Schmid, S. M. (2016). The Exhumation history of the European Alps inferred from linear inversion of thermochronometric data. *Am. J. Sci.* 316, 505–541. doi:10.2475/06.2016.01

Gao, L., Yang, Z., Tong, Y., Wang, H., and An, C. (2015). New paleomagnetic studies of cretaceous and Miocene rocks from jinggu, Western yunnan, China: Evidence for internal deformation of the lanping–simao terrane. *J. Geodyn.* 89, 39–59. doi:10.1016/j.jog.2015.06.004

Ge, Y., Liu-Zeng, J., Zhang, J., Wang, W., Tian, Y., Fox, M., et al. (2020). Spatio-temporal variation in rock exhumation linked to large-scale shear zones in the southeastern Tibetan Plateau. *Sci. China Earth Sci.* 63, 512–532. doi:10.1007/s11430-019-9567-y

Gilley, L. D., Harrison, T. M., Leloup, P. H., Ryerson, F. J., and Wang, J. H. (2003). Direct dating of left-lateral deformation along the Red River shear zone, China and Vietnam. *J. Geophys. Res. Solid Earth* 108. doi:10.1029/2001JB001726

Godard, V., Pik, R., Lavé, J., Cattin, R., Tibari, B., de Sigoyer, J., et al. (2009). Late cenozoic evolution of the central longmen Shan, eastern Tibet: Insight from (U-Th)/He thermochronometry. *Tectonics* 28. doi:10.1029/2008tc002407

Gourbet, L., Yang, R., Fellin, M. G., Paquette, J.-L., Willett, S. D., Gong, J., et al. (2019). Evolution of the Yangtze river network, southeastern Tibet: Insights from thermochronology and sedimentology. *Lithosphere* 12, 3–18. doi:10.1130/l1104.1

Guo, S. (2011). The late Miocene bangmai flora from Lincang county of yunnan, southwestern China. *Acta Paleontol. Sin.* 50, 353–408. doi:10.19800/j.cnki.aps.2011.03.008

Haider, V. L., Dunkl, I., Eynatten, H. V., Ding, L., Frei, D., and Zhang, L. (2013). Cretaceous to cenozoic evolution of the northern Lhasa terrane and the early paleogene development of peneplains at nam Co, Tibetan plateau. *J. Asian Earth Sci.* 71, 79–98. doi:10.1016/j.jseaes.2013.03.005

He, K., He, H., and Cai, H. (1996). Formation and evolution of the Western Yunan orogenic belt. *Geol. Rev.* 42, 97. doi:10.16509/j.georeview.1996.02.001

He, P., Wang, X., Song, C., Wang, Q., Deng, L., and Zhong, S. (2017). Cenozoic evolution of the western qinling Mt. Range based on thermochronologic and sedimentary records from the wudu basin, NE Tibetan plateau. *J. Asian Earth Sci.* 138, 484–494. doi:10.1016/j.jseaes.2017.02.033

Herman, F., and Brandon, M. (2015). Mid-latitude glacial erosion hotspot related to equatorial shifts in southern Westerlies. *Geology* 43, 987–990. doi:10.1130/G37008.1

Herman, F., Seward, D., Valla, P. G., Carter, A., Kohn, B., Willett, S. D., et al. (2013). Worldwide acceleration of mountain erosion under a cooling climate. *Nature* 504, 423–426. doi:10.1038/nature12877

Hetzel, R., Dunkl, I., Haider, V., Strobl, M., Frei, D., Ding, L., et al. (2011). Peneplain formation in southern Tibet predates the India-Asia collision and plateau uplift: Reply. *Geology* 41, e297–e298. doi:10.1130/g34504y.1

Hoke, G. D., Jing, L. Z., Hren, M. T., Wissink, G. K., and Garzione, C. N. (2014). Stable isotopes reveal high southeast Tibetan Plateau margin since the Paleogene. *Earth Planet. Sci. Lett.* 394, 270–278. doi:10.1016/j.epsl.2014.03.007

Houseman, G., and England, P. (1993). Crustal thickening versus lateral expulsion in the Indian-Asian continental collision. *J. Geophys. Res. Solid Earth* 98, 12233–12249. doi:10.1029/93JB00443

Jacques, F. M. B., Guo, S.-X., Su, T., Xing, Y.-W., Huang, Y.-J., Liu, Y.-S., et al. (2011). Quantitative reconstruction of the late Miocene monsoon climates of southwest China: A case study of the Lincang flora from yunnan Province. *Palaeogeogr. Palaeoclimatol. Palaeoecol.* 304, 318–327. doi:10.1016/j.palaeo.2010.04.014

Ji, S., Nie, J., Lechler, A., Huntington, K. W., Heitmann, E. O., and Breecker, D. O. (2018). A symmetrical CO_2 peak and asymmetrical climate change during the middle Miocene. *Earth Planet. Sci. Lett.* 499, 134–144. doi:10.1016/j.epsl.2018.07.011

Jian, X., Guan, P., Zhang, W., Liang, H., Feng, F., and Fu, L. (2018). Late Cretaceous to early Eocene deformation in the northern Tibetan Plateau: Detrital apatite fission track evidence from northern Qaidam basin. *Gondwana Res.* 60, 94–104. doi:10.1016/j.gr.2018.04.007

Jiao, R., Herman, F., and Seward, D. (2017). Late Cenozoic exhumation model of New Zealand: Impacts from tectonics and climate. *Earth-Sci. Rev.* 166, 286–298. doi:10.1016/j.earscirev.2017.01.003

Kapp, P., DeCelles, P. G., Gehrels, G. E., Heizler, M., and Ding, L. (2007). Geological records of the lhasa-qiangtang and indo-asian collisions in the nima area of central Tibet. *Geol. Soc. Am. Bull.* 119, 917–933. doi:10.1130/b26033.1

Kapp, P., Yin, A., Harrison, T. M., and Ding, L. (2005). Cretaceous-Tertiary shortening, basin development, and volcanism in central Tibet. *Geol. Soc. Am. Bull.* 117, 865. doi:10.1130/b25595.1

Kirby, E., Reiners, P. W., Krol, M. A., Whipple, K. X., Hodges, K. V., Farley, K. A., et al. (2002). Late Cenozoic evolution of the eastern margin of the Tibetan Plateau: Inferences from $^{40}Ar/^{39}Ar$ and (U-Th)/He thermochronology. *Tectonics* 21, 1-1–1-20. doi:10.1029/2000TC001246

Kou, X.-Y., Ferguson, D. K., Xu, J.-X., Wang, Y.-F., and Li, C.-S. (2006). The reconstruction of paleovegetation and paleoclimate in the late pliocene of west yunnan, China. *Clim. Change* 77, 431–448. doi:10.1007/s10584-005-9039-5

Lai, Q., Ding, L., Wang, H., Yue, Y., and Cai, F. (2007). Constraining the stepwise migration of the eastern Tibetan Plateau margin by apatite fission track thermochronology. *Sci. China Ser. Earth Sci.* 50, 172–183. doi:10.1007/s11430-007-2048-7

Lei, Y., Zhong, D.-L., Ji, J.-Q., Jia, C., and Zhang, J. (2008). Fission track evidence for two Pleistocene uplift-exhumation events in the eastern Himalayan syntaxis. *Quat. Sci.* 28, 584–590.

Leloup, P. H., Arnaud, N., Lacassin, R., Kienast, J. R., Harrison, T. M., Trong, T. T. P., et al. (2001). New constraints on the structure, thermochronology, and timing of the

Ailao Shan-Red River shear Zone, SE Asia. *J. Geophys. Res. Solid Earth* 106, 6683–6732. doi:10.1029/2000JB900322

Leloup, P. H., Harrison, T. M., Ryerson, F. J., Chen, W., Li, Q., Tapponnier, P., et al. (1993). Structural, petrological and thermal evolution of a tertiary ductile strike-slip-shear zone, diancang Shan, yunnan. *J. Geophys. Res. Solid Earth* 98, 6715–6743. doi:10.1029/92JB02791

Li, G. (1994). A preliminary study of some thrust-nappe structures in Lanping Basin. *Yunnan Geol.*, 203–215.

Li, S.-F., Mao, L.-M., Spicer, R. A., Lebreton-Anberrée, J., Su, T., Sun, M., et al. (2015b). Late Miocene vegetation dynamics under monsoonal climate in southwestern China. *Palaeogeogr. Palaeoclimatol. Palaeoecol.* 425, 14–40. doi:10.1016/j.palaeo.2015.02.030

Li, S., Currie, B. S., Rowley, D. B., and Ingalls, M. (2015a). Cenozoic paleoaltimetry of the SE margin of the Tibetan Plateau: Constraints on the tectonic evolution of the region. *Earth Planet. Sci. Lett.* 432, 415–424. doi:10.1016/j.epsl.2015.09.044

Li, Z.-W., Liu, S., Chen, H., Deng, B., Hou, M., Wu, W., et al. (2012). Spatial variation in Meso-Cenozoic exhumation history of the Longmen Shan thrust belt (eastern Tibetan Plateau) and the adjacent Western Sichuan basin: Constraints from fission track thermochronology. *J. Asian Earth Sci.* 47, 185–203. doi:10.1016/j.jseaes.2011.10.016

Licht, A., van Cappelle, M., Abels, H. A., Ladant, J.-B., Trabucho-Alexandre, J., France-Lanord, C., et al. (2014). Asian monsoons in a late Eocene greenhouse world. *Nature* 513, 501–506. doi:10.1038/nature13704

Lin, T.-H., Lo, C.-H., Chung, S.-L., Hsu, F.-J., Yeh, M.-W., Lee, T.-Y., et al. (2009). $^{40}Ar/^{39}Ar$ dating of the Jiali and Gaoligong shear zones: Implications for crustal deformation around the Eastern Himalayan Syntaxis. *J. Asian Earth Sci.* 34, 674–685. doi:10.1016/j.jseaes.2008.10.009

Liu, F., and Cai, S. (2022). Quantifying the long-term slip rate of Liupan Shan thrust fault through the low-temperature thermochronology. Geol. J. *Gj.* 4587, 209–223. doi:10.1002/gj.4587

Liu, F., Danisik, M., Zheng, D., Gallagher, K., and Nie, J. (2021). Distinguishing tectonic versus climatic forcing on landscape evolution: An example from SE Tibetan Plateau. *Geol. Soc. Am. Bull.* 133, 233–242. doi:10.1130/B35649.1

Liu, S., Zhong, D., and Wu, G. (1998). Jinggu-zhenyuan transpressional basin during continent-continent collision of early tertiary in southwest yunnan, China. *Sci. Geol. Sin.* 2–9.

Liu-Zeng, J., Zhang, J., Ge, Y., Wang, W., Zeng, L., Gen, L., et al. (2018a). Tectonic geomorphology: An interdisciplinary study of the interaction among tectonic climatic and surface processes. *Chin. Sci. Bull.* 63, 3070–3088. doi:10.1360/N972018-00498

Liu-Zeng, J., Zhang, J., Mcphillips, D., Reiners, P., Wang, W., Pik, R., et al. (2018b). Multiple episodes of fast exhumation since Cretaceous in southeast Tibet, revealed by low-temperature thermochronology. *Earth Planet. Sci. Lett.* 490, 62–76. doi:10.1016/j.epsl.2018.03.011

Lu, H., Wang, E., Li, S., and Li, H. (2015). Rotational deformation of the southeastern margin of Tibet: A paleomagnetic study of the yanyuan basin, sichuan Province. *Geol. China* 42, 1188–1201.

Molnar, P., England, P., and Martinod, J. (1993). Mantle dynamics, uplift of the Tibetan plateau, and the Indian monsoon. *Rev. Geophys.* 31, 357–396. doi:10.1029/93RG02030

Molnar, P. (2005). The growth of the Tibetan Plateau and Mio-Pliocene evolution of East Asian climate. *Palaeontol. Electron.* 8, 1–23. doi:10.1016/j.palaeo.2009.11.002

Molnar, P., and Tapponnier, P. (1975). Cenozoic Tectonics of Asia: Effects of a Continental Collision: Features of recent continental tectonics in Asia can be interpreted as results of the India-Eurasia collision. *Science* 189, 419–426. doi:10.1126/science.189.4201.419

Murphy, M. A., Yin, A., Harrison, T. M., Dürr, S. B., Ryerson, F. J., et al. (1997). Did the Indo-Asian collision alone create the Tibetan plateau? *Geology* 25, 719. doi:10.1130/0091-7613(1997)025<0719:DTIACA>2.3.CO;2

Nie, J., Ruetenik, G., Gallagher, K., Hoke, G., Garzione, C. N., Wang, W., et al. (2018). Rapid incision of the Mekong River in the middle Miocene linked to monsoonal precipitation. *Nat. Geosci.* 11, 944–948. doi:10.1038/s41561-018-0244-z

Ou, X., Replumaz, A., and van der Beek, P. (2020). Contrasting exhumation histories and relief development within the three rivers region (southeast Tibet). *Solid earth*. doi:10.5194/se-2020-172

Ouimet, W., Whipple, K., Royden, L., Reiners, P., Hodges, K., and Pringle, M. (2010). Regional incision of the eastern margin of the Tibetan Plateau. *Lithosphere* 2, 50–63. doi:10.1130/L57.1

Pan, Y., and Shen, W. B. (2017). Contemporary crustal movement of southeastern Tibet: Constraints from dense GPS measurements. *Sci. Rep.* 7, 45348. doi:10.1038/srep45348

Pei, J., Tong, Y., Pu, Z., Jing, X., Cai, Y., Li, J., et al. (2019). Towards artificial general intelligence with hybrid Tianjic chip architecture. *Acta Geosci. Sin.* 40, 106–111. doi:10.1038/s41586-019-1424-8

Polissar, P. J., Freeman, K. H., Rowley, D. B., Mcinerney, F. A., and Currie, B. S. (2009). Paleoaltimetry of the Tibetan Plateau from D/H ratios of lipid biomarkers. *Earth Planet. Sci. Lett.* 287, 64–76. doi:10.1016/j.epsl.2009.07.037

Powell, C. M. (1986). Continental underplating model for the rise of the Tibetan Plateau. *Earth Planet. Sci. Lett.* 81, 79–94. doi:10.1016/0012-821X(86)90102-0

Prell, W. L., and Kutzbach, J. E. (1992). Sensitivity of the Indian monsoon to forcing parameters and implications for its evolution. *Nature* 360, 647–652. doi:10.1038/360647a0

Reiners, P. W. (2007). Thermochronologic approaches to paleotopography. *Rev. Mineral. Geochem.* 66, 243–267. doi:10.2138/rmg.2007.66.10

Ren, L., Zhang, B., Zheng, D.-W., Wang, Y., Zhang, J., Li, X., et al. (2020a). Tectonic transformation and its exhumation history of the Ailao Shan-Red River shear zone in Oligocene: Evidences from apatite fission track thermochronology of the southern segment of the Ailao Shan range. *Acta Petrol. Sin.* 36, 1787–1802. doi:10.18654/1000-0569/2020.06.09

Ren, X., Nie, J., Saylor, J. E., Wang, X., Liu, F., and Horton, B. K. (2020b). Temperature control on silicate weathering intensity and evolution of the Neogene east Asian summer monsoon. *Geophys. Res. Lett.* 47, e2020GL088808. doi:10.1029/2020GL088808

Replumaz, A., San José, M., Margirier, A., Beek, P., Gautheron, C., Leloup, P. H., et al. (2020). Tectonic control on rapid late-miocene-quaternary incision of the mekong river knickzone, southeast Tibetan plateau. *Tectonics* 39. doi:10.1029/2019tc005782

Roger, F., Calassou, S., Lancelot, J., Malavieille, J., Mattauer, M., Zhiqin, X., et al. (1995). Miocene emplacement and deformation of the Konga Shan granite (Xianshui He fault zone, west Sichuan, China): Geodynamic implications. *Earth Planet. Sci. Lett.* 130, 201–216. doi:10.1016/0012-821X(94)00252-T

Rohrmann, A., Kapp, P., Carrapa, B., Reiners, P. W., Guynn, J., Ding, L., et al. (2012). Thermochronologic evidence for plateau formation in central Tibet by 45 Ma. *Geology* 40, 187–190. doi:10.1130/G32530.1

Rowley, D. B., and Currie, B. S. (2006). Palaeo-altimetry of the late Eocene to Miocene lunpola basin, central Tibet. *Nature* 439, 677–681. doi:10.1038/nature04506

Royden, L. H., Burchfiel, B. C., King, R. W., Wang, E., Chen, Z., Shen, F., et al. (1997). Surface deformation and lower crustal flow in eastern Tibet. *Science* 276, 788–790. doi:10.1126/science.276.5313.788

Shen, F., Royden, L. H., and Burchfiel, B. C. (2001). Large-scale crustal deformation of the Tibetan Plateau. *J. Geophys. Res. Solid Earth* 106, 6793–6816. doi:10.1029/2000JB900389

Shen, X., Tian, Y., Li, D., Qin, S., Vermeesch, P., and Schwanethal, J. (2016). Oligocene-Early Miocene river incision near the first bend of the Yangze River: Insights from apatite (U-Th-Sm)/He thermochronology. *Tectonophysics* 687, 223–231. doi:10.1016/j.tecto.2016.08.006

Shen, X., Tian, Y., Wang, Y., Wu, L., Jia, Y., Tang, X., et al. (2021). Enhanced quaternary exhumation in the central three rivers region, southeastern Tibet. *Front. Earth Sci.* 9, 741491. doi:10.3389/feart.2021.741491

Shen, X., Tian, Y., Zhang, G., Zhang, S., Carter, A., Kohn, B., et al. (2019). Late Miocene hinterland crustal shortening in the Longmen Shan thrust belt, the eastern margin of the Tibetan Plateau. *J. Geophys. Res. Solid Earth* 124, 11972–11991. doi:10.1029/2019jb018358

Shi, X., Qiu, X., Liu, H., Chu, Z., and Xia, B. (2006). Thermochronological analyses on the cooling history of the Lincang granitoid batholith, western yunnan. *Acta Petrol. Sin.* 22, 465–479.

Siravo, G., Faccenna, C., Gérault, M., Becker, T. W., Fellin, M. G., Herman, F., et al. (2019). Slab flattening and the rise of the eastern cordillera, Colombia. *Earth Planet. Sci. Lett.* 512, 100–110. doi:10.1016/j.epsl.2019.02.002

Stalder, N. F., Herman, F., Fellin, M. G., Coutand, I., Aguilar, G., Reiners, P. W., et al. (2020). The relationships between tectonics, climate and exhumation in the Central Andes (18–36°S): Evidence from low-temperature thermochronology. *Earth-Sci. Rev.* 210, 103276. doi:10.1016/j.earscirev.2020.103276

Sun, B.-N., Wu, J.-Y., Liu, Y.-S., Ding, S.-T., Li, X.-C., Xie, S.-P., et al. (2011). Reconstructing Neogene vegetation and climates to infer tectonic uplift in Western Yunnan, China. *Palaeogeogr. Palaeoclimatol. Palaeoecol.* 304, 328–336. doi:10.1016/j.palaeo.2010.09.023

Tan, X., Lee, Y.-H., Chen, W.-Y., Cook, K. L., and Xu, X.-W. (2014). Exhumation history and faulting activity of the southern segment of the Longmen Shan, eastern Tibet. *J. Asian Earth Sci.* 81, 91–104. doi:10.1016/j.jseaes.2013.12.002

Tan, X., Liu, Y., Lee, Y.-H., Lu, R., Xu, X., Suppe, J., et al. (2019). Parallelism between the maximum exhumation belt and the Moho ramp along the eastern Tibetan Plateau margin: Coincidence or consequence? *Earth Planet. Sci. Lett.* 507, 73–84. doi:10.1016/j.epsl.2018.12.001

Tan, X., Xu, X.-W., Lee, Y.-H., Lu, R.-Q., Liu, Y., Xu, C., et al. (2017). Late Cenozoic thrusting of major faults along the central segment of Longmen Shan, eastern Tibet: Evidence from low-temperature thermochronology. *Tectonophysics* 712–713, 145–155. doi:10.1016/j.tecto.2017.05.016

Tapponnier, P., Mercier, J. L., Armijo, R., Tonglin, H., and Ji, Z. (1981). Field evidence for active normal faulting in Tibet. *Nature* 294, 410–414. doi:10.1038/294410a0

Tapponnier, P., Zhiqin, X., Roger, F., Meyer, B., Arnaud, N., Wittlinger, G., et al. (2001). Oblique stepwise rise and growth of the Tibet plateau. *Science* 294, 1671–1677. doi:10.1126/science.105978

Tian, Y., Kohn, B. P., Gleadow, A. J. W., and Hu, S. (2014). A thermochronological perspective on the morphotectonic evolution of the southeastern Tibetan Plateau. *J. Geophys. Res. Solid Earth.* 119, 676–698. doi:10.1002/2013JB010429

Tian, Y., Kohn, B. P., Gleadow, A. J. W., and Hu, S. (2013). Constructing the Longmen Shan eastern Tibetan Plateau margin: Insights from low-temperature thermochronology. *Tectonics* 32, 576–592. doi:10.1002/tect.20043

Tian, Y., Kohn, B. P., Hu, S., and Gleadow, A. J. W. (2015). Synchronous fluvial response to surface uplift in the eastern Tibetan Plateau: Implications for crustal dynamics. *Geophys. Res. Lett.* 42, 29–35. doi:10.1002/2014GL062383

Tian, Y., Li, R., Tang, Y., Xu, X., Wang, Y., and Zhang, P. (2018). Thermochronological constraints on the late cenozoic morphotectonic evolution of the Min Shan, the eastern margin of the Tibetan plateau. *Tectonics* 37, 1733–1749. doi:10.1029/2017tc004868

Tong, Y.-B., Yang, Z., Zheng, L.-D., Xu, Y.-L., Wang, H., Gao, L., et al. (2013). Internal crustal deformation in the northern part of Shan-Thai Block: New evidence from paleomagnetic results of Cretaceous and Paleogene redbeds. *Tectonophysics* 608, 1138–1158. doi:10.1016/j.tecto.2013.06.031

Tong, Y., Yang, Z., Jing, X., Zhao, Y., Li, C., Huang, D., et al. (2016). New insights into the Cenozoic lateral extrusion of crustal blocks on the southeastern edge of Tibetan Plateau: Evidence from paleomagnetic results from Paleogene sedimentary strata of the Baoshan Terrane. *Tectonics* 35, 2494–2514. doi:10.1002/2016TC004221

Tsuchiyama, Y., Zaman, H., Sotham, S., Samuth, Y., Sato, E., Ahn, H.-S., et al. (2016). Paleomagnetism of late jurassic to early cretaceous red beds from the cardamom mountains, southwestern Cambodia: Tectonic deformation of the Indochina peninsula. *Earth Planet. Sci. Lett.* 434, 274–288. doi:10.1016/j.epsl.2015.11.045

Turner, S., Hawkesworth, C., Liu, J., Rogers, N., Kelley, S., and Calsteren, P. V. (1993). Timing of Tibetan uplift constrained by analysis of volcanic rocks. *Nature* 364, 50–54. doi:10.1038/364050a0

Vermeesch, P. (2012). On the visualisation of detrital age distributions. *Chem. Geol.* 312–313, 190–194. doi:10.1016/j.chemgeo.2012.04.021

Wang, C., Dai, J., Zhao, X., Li, Y., Graham, S. A., He, D., et al. (2014). Outward-growth of the Tibetan Plateau during the cenozoic: A review. *Tectonophysics* 621, 1–43. doi:10.1016/j.tecto.2014.01.036

Wang, E., and Burchfiel, B. C. (1997). Interpretation of cenozoic tectonics in the right-lateral accommodation zone between the Ailao Shan shear zone and the eastern himalayan syntaxis. *Int. Geol. Rev.* 39, 191–219. doi:10.1080/00206819709465267

Wang, E., Kirby, E., Furlong, K. P., Soest, M. V., Xu, G., Shi, X., et al. (2012a). Two-phase growth of high topography in eastern Tibet during the Cenozoic. *Nat. Geosci.* 5, 640–645. doi:10.1038/ngeo1538

Wang, G., Wan, J., Wang, E., Zheng, D., and Li, F. (2008). Late Cenozoic to recent transtensional deformation across the Southern part of the Gaoligong shear zone between the Indian plate and SE margin of the Tibetan plateau and its tectonic origin. *Tectonophysics* 460, 1–20. doi:10.1016/j.tecto.2008.04.007

Wang, H., Tian, Y., and Liang, M. (2017). Late cenozoic exhumation history of the luoji Shan in the southeastern Tibetan plateau: Insights from apatite fission-track thermochronology. *JGS* 174, 883–891. doi:10.1144/jgs2017-005

Wang, M., and Shen, Z. (2020). Present-day crustal deformation of continental China derived from GPS and its tectonic implications. *J. Geophys. Res. Solid Earth* 125. doi:10.1029/2019JB018774

Wang, S., Fang, X., Zheng, D., and Wang, E. (2009). Initiation of slip along the Xianshuihe fault zone, eastern Tibet, constrained by K/Ar and fission-track ages. *Int. Geol. Rev.* 51, 1121–1131. doi:10.1080/00206810902945132

Wang, S., Jiang, G., Xu, T., Tian, Y., Zheng, D., and Fang, X. (2012b). The jinhe–qinghe fault—an inactive branch of the xianshuihe–xiaojiang fault zone, eastern Tibet. *Tectonophysics* 544–545, 93–102. doi:10.1016/j.tecto.2012.04.004

Wang, Y., Fan, W., Zhang, Y., Peng, T., Chen, X., and Xu, Y. (2006). Kinematics and $^{40}Ar/^{39}Ar$ geochronology of the Gaoligong and Chongshan shear systems, Western Yunnan, China: Implications for early Oligocene tectonic extrusion of SE Asia. *Tectonophysics* 418, 235–254. doi:10.1016/j.tecto.2006.02.005

Wang, Y., Mei, G., Xie, Q., Zhou, X., and Wang, G. (2015). Apatite fission track evidence for the Cenozoic uplift process in Garze area on the eastern margin of the Tibetan Plateau. *Geol. China* 42, 469–479.

Wang, Y., Wang, Y., Zhang, P., Schoenbohm, L. M., Zhang, B., Zhang, J., et al. (2019). Intracontinental deformation within the India-Eurasia oblique convergence zone: Case studies on the Nantinghe and Dayingjiang faults. *GSA Bull.* 132, 850–862. doi:10.1130/b35338.1

Wang, Y., Zhang, B., Schoenbohm, L. M., Zhang, J., Zhou, R., Hou, J., et al. (2016). Late Cenozoic tectonic evolution of the Ailao Shan-Red River fault (SE Tibet): Implications for kinematic change during plateau growth. *Tectonics* 35, 1969–1988. doi:10.1002/2016tc004229

Wang, Y., Zhang, P., Schoenbohm, L. M., Zheng, W., Zhang, B., Zhang, J., et al. (2018). Two-phase exhumation along major shear zones in the SE Tibetan plateau in the late cenozoic. *Tectonics* 37, 2675–2694. doi:10.1029/2018tc004979

Willett, S. D., Herman, F., Fox, M., Stalder, N., Ehlers, T. A., Jiao, R., et al. (2020). *Bias and error in modelling thermochronometric data: Resolving a potential increase in plio-pleistocene erosion rate. Cross-Cutting themes: Geochronology applied to establish timing and rates of earth surface processes*. doi:10.5194/esurf-2020-59

Wu, G. (1994). Tertiary thrusting-nappe structures in northwest Yunnan, China. *Geotecton. Metallog.*, 331–338. doi:10.16539/j.ddgzyckx.1994.04.006

Wu, J., Zhang, K., Xu, Y., Wang, G., Garzione, C. N., Eiler, J., et al. (2018). Paleoelevations in the Jianchuan Basin of the southeastern Tibetan Plateau based on stable isotope and pollen grain analyses. *Palaeogeogr. Palaeoclimatol. Palaeoecol.* 510, 93–108. doi:10.1016/j.palaeo.2018.03.030

Xia, K., Su, T., Liu, Y.-S., Xing, Y.-W., Jacques, F. M. B., and Zhou, Z.-K. (2009). Quantitative climate reconstructions of the late Miocene Xiaolongtan megaflora from Yunnan, southwest China. *Palaeogeogr. Palaeoclimatol. Palaeoecol.* 276, 80–86. doi:10.1016/j.palaeo.2009.02.024

Xiao, P., Liu-Zeng, J., Wang, W., Zeng, L., Xie, K., Pik, R., et al. (2015). The thermal history of the Baimaxueshan pluton in Deqin area and its implications for the tectonic-geomorphic evolution in the Three River Region of Tibetan Plateau. *Acta Petrol. Sin.* 31, 1348–1360.

Xing, Y., Utescher, T., Jacques, F. M. B., Su, T., Liu, Y., Huang, Y., et al. (2012). Paleoclimatic estimation reveals a weak winter monsoon in southwestern China during the late Miocene: Evidence from plant macrofossils. *Palaeogeogr. Palaeoclimatol. Palaeoecol.* 358–360, 19–26. doi:10.1016/j.palaeo.2012.07.011

Xu, J.-X., Ferguson, D. K., Li, C.-S., and Wang, Y.-F. (2008). Late Miocene vegetation and climate of the Lühe region in Yunnan, southwestern China. *Rev. Palaeobot. Palynol.* 148, 36–59. doi:10.1016/j.revpalbo.2007.08.004

Xu, J. (2002). *Palynology, paleovegetation and paleoclimate of Neogene central-western yunnan, China*. Doctoral thesis, Institute of Botany, Chinese Academy of Sciences.

Yang, R., Fellin, M. G., Herman, F., Willett, S. D., Wang, W., and Maden, C. (2016). Spatial and temporal pattern of erosion in the three rivers region, southeastern Tibet. *Earth Planet. Sci. Lett.* 433, 10–20. doi:10.1016/j.epsl.2015.10.032

Yang, R., Suhail, H. A., Gourbet, L., Willett, S. D., Fellin, M. G., Lin, X., et al. (2020a). Early Pleistocene drainage pattern changes in Eastern Tibet: Constraints from provenance analysis, thermochronometry, and numerical modeling. *Earth Planet. Sci. Lett.* 531, 115955. doi:10.1016/j.epsl.2019.115955

Yang, X., Tong, Y., Wang, H., Pei, J., Sun, Xi., Wang, C., et al. (2020b). The contributing factor of differential crustal deformation of the Lanping-Simao terrane in the southeastern edge of the Xizang (Tibetan) Plateau since late Eocene. *Geol. Rev.* 66, 853–873. doi:10.16509/j.georeview.2020.04.005

Yang, Z. Y., Besse, J., Sutheetorn, V., Bassoullet, J. P., Fontaine, H., and Buffetaut, E. (1995). Lower-middle jurassic paleomagnetic data from the mae sot area (Thailand): Paleogeographic evolution and deformation history of southeastern Asia. *Earth Planet. Sci. Lett.* 136, 325–341. doi:10.1016/0012-821X(95)00192-F

Yin, A., and Harrison, T. M. (2000). Geologic evolution of the himalayan-Tibetan orogen. *Annu. Rev. Earth Planet. Sci.* 28, 211–280. doi:10.1146/annurev.earth.28.1.211

Zhang, G., Tian, Y., Li, R., Shen, X., Zhang, Z., Sun, X., et al. (2022). Progressive tectonic evolution from crustal shortening to mid-lower crustal expansion in the southeast Tibetan plateau: A synthesis of structural and thermochronological insights. *Earth-Sci. Rev.* 226, 103951. doi:10.1016/j.earscirev.2022.103951

Zhang, H., Oskin, M. E., Liuzeng, J., Zhang, P., Reiners, P. W., and Xiao, P. (2016). Pulsed exhumation of interior eastern Tibet: Implications for relief generation mechanisms and the origin of high-elevation planation surfaces. *Earth Planet. Sci. Lett.* 449, 176–185. doi:10.1016/j.epsl.2016.05.048

Zhang, Y.-Z., Replumaz, A., Leloup, P. H., Wang, G.-C., Bernet, M., van der Beek, P., et al. (2017). Cooling history of the Gongga batholith: Implications for the Xianshuihe fault and Miocene kinematics of SE Tibet. *Earth Planet. Sci. Lett.* 465, 1–15. doi:10.1016/j.epsl.2017.02.025

Zhang, Y.-Z., Replumaz, A., Wang, G.-C., Leloup, P. H., Gautheron, C., Bernet, M., et al. (2015). Timing and rate of exhumation along the Litang fault system, implication for fault reorganization in Southeast Tibet. *Tectonics* 34, 1219–1243. doi:10.1002/2014TC003671

Zhao, W. L., and Morgan, W. J. (1987). Injection of Indian crust into Tibetan lower crust: A two-dimensional finite element model study. *Tectonics* 6, 489–504. doi:10.1029/tc006i004p00489

Zhu, R. X., Potts, R., Pan, Y. X., Lü, L. Q., Yao, H. T., Deng, C. L., et al. (2008). Paleomagnetism of the Yuanmou Basin near the southeastern margin of the Tibetan Plateau and its constraints on late Neogene sedimentation and tectonic rotation. *Earth Planet. Sci. Lett.* 272, 97–104. doi:10.1016/j.epsl.2008.04.016

Zou, B., Wang, G., and Deng, J. (2014). Evidence for apatite fission track of Pliocene rapid uplift of Zhongdian region on southeastern margin of Tibetan Plateau, China. *J. Chengdu Univ. Technol. Technol. Ed.* 41, 227–236. doi:10.3969/j.issn.1671-9727.2014.02.12